iScience

CellPress
OPEN ACCESS

Article

Autosomal recessive variants in *TUBGCP2* alter the γ-tubulin ring complex leading to neurodevelopmental disease

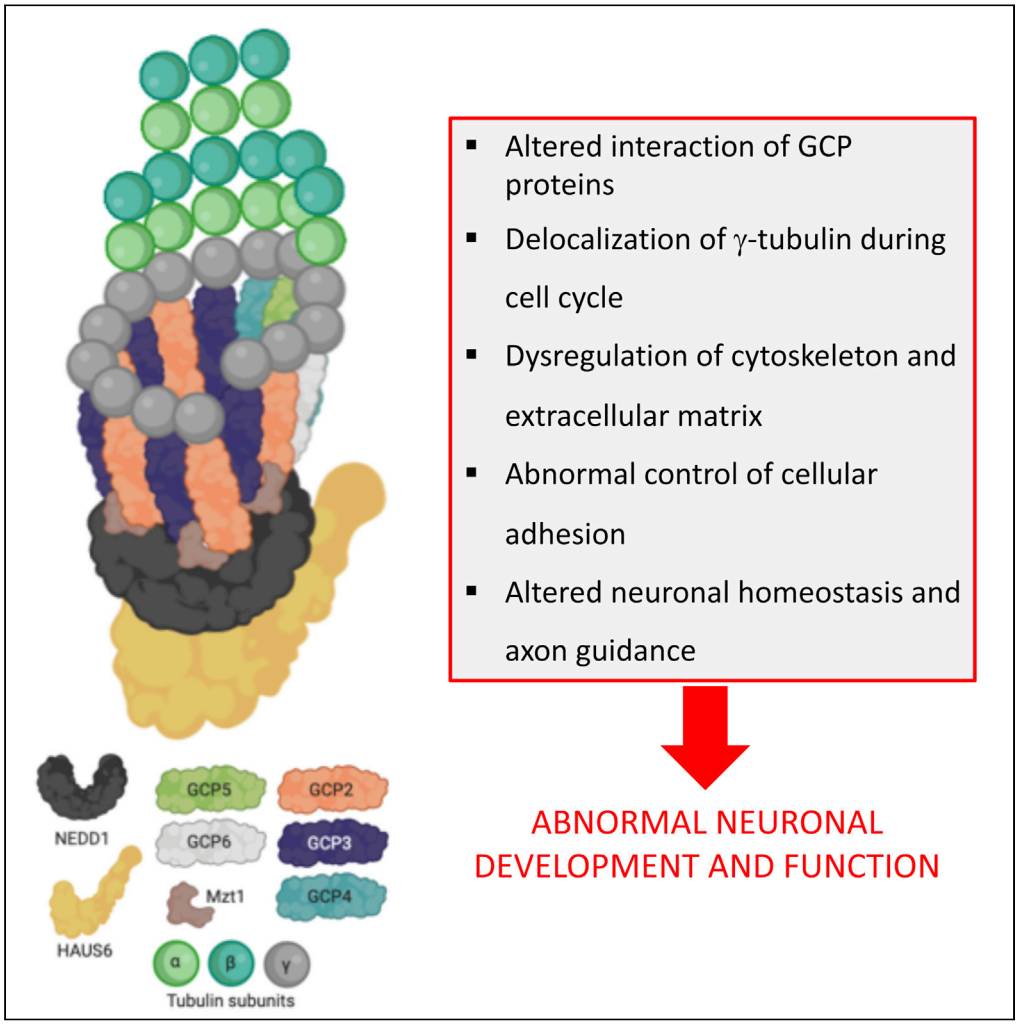

Serdal Gungor, Yavuz Oktay, Semra Hiz, ..., Hanns Lochmuller, Isabelle Vernos, Rita Horvath

rh732@medschl.cam.ac.uk

Highlights

TUBGCP2 variants cause neurodevelopmental delay, brain malformation, and epilepsy

The variant alters GCP2/GCP3 interaction and localization of GCP2 in cell cycle

We link GCP2 to the cytoskeleton, extracellular matrix, cell adhesion, and axon guidance

Functional proteomics is useful in establishing molecular pathways in rare diseases

Gungor et al., iScience *24*, 101948
January 22, 2021
https://doi.org/10.1016/j.isci.2020.101948

iScience

CellPress
OPEN ACCESS

Article

Autosomal recessive variants in *TUBGCP2* alter the γ-tubulin ring complex leading to neurodevelopmental disease

Serdal Gungor,[1,17] Yavuz Oktay,[2,3,17] Semra Hiz,[2,4,17] Álvaro Aranguren-Ibáñez,[5,17] Ipek Kalafatcilar,[2,4] Ahmet Yaramis,[6] Ezgi Karaca,[2,3] Uluc Yis,[4] Ece Sonmezler,[2] Burcu Ekinci,[2] Mahmut Aslan,[4] Elmasnur Yilmaz,[2] Bilge Özgör,[1] Sunitha Balaraju,[7,8] Nora Szabo,[8,9] Steven Laurie,[10] Sergi Beltran,[10] Daniel G. MacArthur,[11,12] Denisa Hathazi,[8] Ana Töpf,[7] Andreas Roos,[13,17] Hanns Lochmuller,[14,17] Isabelle Vernos,[5,15,16,17] and Rita Horvath[7,17,18,*]

Summary

Microtubules help building the cytoskeleton of neurons and other cells. Several components of the gamma-tubulin (γ-tubulin) complex have been previously reported in human neurodevelopmental diseases. We describe two siblings from a consanguineous Turkish family with dysmorphic features, developmental delay, brain malformation, and epilepsy carrying a homozygous mutation (p.Glu311Lys) in *TUBGCP2* encoding the γ-tubulin complex 2 (GCP2) protein. This variant is predicted to disrupt the electrostatic interaction of GCP2 with GCP3. In primary fibroblasts carrying the variant, we observed a faint delocalization of γ-tubulin during the cell cycle but normal GCP2 protein levels. Through mass spectrometry, we observed dysregulation of multiple proteins involved in the assembly and organization of the cytoskeleton and the extracellular matrix, controlling cellular adhesion and of proteins crucial for neuronal homeostasis including axon guidance. In summary, our functional and proteomic studies link TUBGCP2 and the γ-tubulin complex to the development of the central nervous system in humans.

Introduction

Microtubules (MTs) are dynamic, cytoskeletal polymers crucial for cortical development and neuronal migration. Mutations in several genes encoding alpha-tubulin (*TUBA1A*), beta-tubulin (*TUBB2A*, *TUBB2B*, *TUBB3*, *TUBB4A*, *TUBB*), and gamma-tubulin (γ-tubulin) (*TUBG1*) isoforms have been associated with a wide range of brain malformations including lissencephaly, polymicrogyria, microlissencephaly, and simplified gyration (Romaniello et al., 2018). Mutations in different tubulin genes cause various phenotypes (Table 1). Alpha-tubulin and γ-tubulin gene mutations predominantly result in lissencephaly spectrum diseases (Romaniello et al., 2018). Beta-tubulin gene mutations may show normal cortical pattern; however, *TUBB4A* is predominantly associated with hypomyelination and cerebellar and brainstem atrophy (Blumkin et al., 2014). *TUBB2B* and *TUBB3* mutations seem to be more related to polymicroglial patterns. Microcephaly and ocular malformations are commonly seen in beta-tubulin (TUBB) defects (Francis and Belvindrah, 2018; Romaniello et al., 2018).

Mutations in several components of the γ-tubulin complex including *TUBGCP4*, *TUBGCP5*, and *TUBGCP6* have been previously reported in human neurodevelopmental diseases often associated with microcephaly (Maver et al., 2019; Mitani et al., 2019; Scheidecker et al., 2015) (Da Palma et al., 2020; Hull et al., 2019; Maver et al., 2019; Mitani et al., 2019). Most of these mutations led to a loss of function and reduced levels of several GCP proteins (Table 1). Autosomal recessive variants in *TUBGCP2* encoding the γ-tubulin complex 2 (GCP2) protein were first reported in 5 individuals from 4 families with developmental delay, dysmorphic features, hypotonia, epilepsy, microcephaly, and lissencephaly spectrum changes on brain magnetic resonance imaging (pachygyria, agyria, subcortical band heterotopia), representing defective neuronal migration (Mitani et al., 2019). Thin corpus callosum, cerebellar and pons atrophy, and white matter abnormalities were also reported in some cases (Table 2). The authors speculated that the clinical phenotype was possibly

[1]Inonu University, Faculty of Medicine, Turgut Ozal Research Center, Department of Paediatric Neurology, Malatya, Turkey

[2]Izmir Biomedicine and Genome Center, Dokuz Eylul University Health Campus, Izmir, Turkey

[3]Department of Medical Biology, Faculty of Medicine, Dokuz Eylul University and Izmir International Biomedicine and Genome Institute, Dokuz Eylul University, Izmir, Turkey

[4]Dokuz Eylul University, Faculty of Medicine, Department of Pediatric Neurology Izmir, Turkey

[5]Centre for Genomic Regulation (CRG), the Barcelona Institute of Science and Technology, Dr. Aiguader 88, Barcelona 08003, Spain

[6]Pediatric Neurology Clinic, Private Office, Diyarbakir, Turkey

[7]John Walton Muscular Dystrophy Research Centre, Institute of Translational and Clinical Research, Newcastle University, Newcastle upon Tyne, UK

[8]Department of Clinical Neurosciences, John Van Geest Cambridge Centre for Brain Repair, University of Cambridge School of Clinical Medicine, Robinson Way, Cambridge CB2 0PY, UK

[9]Budai Children Hospital, Észak-Közép-budai Centrum, Új Szent János Kórház és Szakrendelő, Budapest, Hungary

[10]CNAG-CRG, Centre for Genomic Regulation,

Continued

due to a disturbed binding of different proteins to γ-tubulin or altered interactions between γ-tubulin complex proteins. However, no supporting functional data were provided that could shed light on the impact of these disease-causing variants on the mutant protein.

MTs are one of the main cytoskeleton builders and are involved in many important functions such as intracellular transport, organelle positioning, motility, signaling, and cell division (Brouhard and Rice, 2018; Vale, 2003). MTs are long fibers of 25 nm in diameter made of 13 polarized protofilaments in mammals, each protofilament composed of α- and β-tubulin heterodimers (de Pablo et al., 2003). The polarity of the tube provides specific dynamic characteristics to the ends where different polymerization and depolymerization reactions occur (Brouhard and Rice, 2018). MTs are mainly formed at the MT organizing centers (MTOCs), the centrosome being the most important MTOC in mammals (Wu and Akhmanova, 2017). Centrosomes are organelles composed of two perpendicular barrels of 9 triplets of MTs surrounded by a proteinaceus matrix called the pericentriolar material (PCM) (Fry et al., 2017). Cryo-electron microscopy studies on structure of the human γTuRC, combined with cross-linking mass spectrometry analysis, reveal an asymmetric conformation with only part of the complex in a "closed" conformation, while the opposite side of γTuRC is in an "open" conformation, leading to a structural asymmetry suggesting possible regulatory mechanisms for MT nucleation by γTuRC closure (Consolati et al., 2020; Rale et al., 2018). This complex named γ-tubulin ring complex or γ-TuRC was found to work as an MT nucleation complex (Tovey and Conduit, 2018). Further biochemical analysis identified at least seven proteins co-purifying with γ-tubulin in mammalian cells, known as γ-tubulin complex proteins or GCPs (GCP2-6) (Yu et al., 2016). One molecule of GCP2 together with one molecule of GCP3 and two molecules of γ-tubulin form a γ-tubulin small complex or γ-TuSC, the basic unit of the γ-TuRC (Raynaud-Messina and Merdes, 2007). A full γ-TuRC consists of several γ-TuSC associated with a few additional GCPs. In addition to its nucleating activity, the γ-TuRC also acts as a minus-end capping complex, therefore stabilizing MTs.

The γ-TuRC is targeted to the centrosome through the neural precursor cell expressed developmentally down-regulated protein 1 (NEDD1). The N-terminal part of NEDD1 contains a conserved WD40 domain necessary for centrosome binding, while the C-terminal part is required for γ-tubulin interaction (Yonezawa et al., 2015). Different phosphorylations in NEDD1 control not only the targeting of γ-TuRC to the centrosome but also the spatial and temporal regulation of MT nucleation at different sites in the cell (Gomez-Ferreria et al., 2012). For instance, a recently described mechanism explains acentrosomal MT assembly in mitosis by an octameric complex of proteins termed the Augmin complex. This eight-subunit complex is conserved in animal and plants and is composed of the HAUS proteins (HAUS1-8). HAUS6 binds to γ-TuRC while HAUS8 directly binds to the lattice of a pre-existing MT, creating an MT nucleation point and, thus, an MT branching point (Lawo et al., 2009).

In this report, we studied the localization of several components of the γ-TuRC complex in control and *TUBGCP2* mutated human fibroblasts, as well as the levels of the TUBGCP2 protein along the cell cycle, and performed proteomics and structural modeling studies to explore the functional effect of the mutant TUBGCP2 protein in neurodegeneration.

Results

Patients

We studied 2 siblings born to consanguineous Turkish parents. Patients and family members were recruited at the Department of Paediatric Neurology, Malatya (Turkey) after informed consent. Samples were pseudo-anonymized, processed, and stored within the MRC Centre for Neuromuscular Diseases Biobank (National Research Ethics Service, Newcastle and North Tyneside 1 Research Ethics Committee: REC reference number 08/H0906/28 + 5).

The 10-year-old female patient was the second child born to first cousin parents (Figure 1A). She presented with severe developmental delay, hypotonia, and intractable epilepsy at age 6 months and lost all motor and cognitive abilities gradually by 4 years of age. She presented dysmorphic features including narrow forehead, thick eyebrows, bulbous nose, prominent ear, widely separated teeth, retrognathia, and maxillary hypoplasia (Table 2, Figure 1B). Neurological examination revealed microcephaly, atrophy, and contractures of the extremities with brisk deep tendon reflexes and spasticity. Cranial T2-weighted magnetic resonance (MR) images showed pachygyria, cerebellar parenchymal atrophy, bilateral volume loss in cerebral white matter, cystic foci with increased intensity in the neighboring white matter, and thinning of the

Barcelona Institute of Science and Technology, Barcelona, Spain

[11]Analytic and Translational Genetics Unit, Massachusetts General Hospital, Boston, MA, USA

[12]Program in Medical and Population Genetics, Broad Institute of MIT and Harvard, Cambridge, MA, USA

[13]Leibniz Institut für Analytische Wissenschaften, ISAS, Dortmund, Germany & Pediatric Neurology, University Hospital, University of Duisburg-Essen, Faculty of Medicine, Essen, Germany

[14]Children's Hospital of Eastern Ontario Research Institute; Division of Neurology, Department of Medicine, the Ottawa Hospital; and Brain and Mind Research Institute, University of Ottawa, Ottawa, Canada

[15]Universitat Pompeu Fabra (UPF), Barcelona, Spain

[16]Institució Catalana de Recerca i Estudis Avançats (ICREA), Spain

[17]These authors contributed equally

[18]Lead Contact

*Correspondence: rh732@medschl.cam.ac.uk

https://doi.org/10.1016/j.isci.2020.101948

Table 1. Functional effect and clinical phentotype of pathogenic mutations in tubulin complex protein genes

Function	Gene	Variants (nucleotide/ protein/zygosity)	Effects		Severity	Clinical features	Common MRI findings (# of positive cases/ # of total cases)
ɣ-TuSC and ɣ-TuRC genes (except ɣ-tubulins)	TUBGCP2	c.1015G > A, p.Glu311Lys, Hom	Changes in TUBGCP2, HAUS6, NEDD1 protein localizations in mitosis/no change in GCP2 level		Severe or moderate	DD ID Facial dysmorphism Hypotonia	Pachygyria (7/7) Thin CC (6/7) Cerebellar atrophy(5/7) WM volume loss (3/7) Brainstem atrophy (2/7) Subcrotical band (2/7) WM hyperintensity with subependimal cysts (4/7)
		c.997C > T, p.Arg333Cys, Hom[a]	Alteration in the part of the conserved Grip1 domain		Severe (2q23.1 dup) or moderate		
		c.1843G > C, p.Ala615Pro, Hom[a]	Changes in the Grip2 domain		Severe		
		c.889C > T, p.Arg297Cys c.2025-2A > G, Cmp Het[a]	Changes in the extended conserved Grip1 domain Alternative splice acceptor site; excision of exon 15 or inclusion of intron 13 and premature stop codon		Mild		
	TUBGCP4	c.1746G > T, p.Leu582 =,Cmp Het[b]	Alternative splice acceptor site; exon 16 skipping	Truncated GCP4 protein and reduced amounts of GCP4 and other proteins; GCP2, GCP5, GCP6, ɣ-tubulin in interphase and in mitosis, reduced levels of ɣ-TuRC		Congenital microcephaly Chorioretinopathy (MCCRP) ID Facial dysmorphism	Thin CC (1/5) Normal (4/5) No cortical malformation
		c.1746G > T + c.579dupT, p.Gly194Trpfs*8[b]	Frameshift mutation		Moderate (thin CC and ID)		
		c.1746G > T + c.298delT, p.Tyr100Ilefs*27[b]	Frameshift mutation		Mild		
		c.1746G > T + c.1732-?_ *544+?del[b]	Exon 16-18 del, ~544 nucleotide del of 3′ UTR		Mild		
		c.1746G > T + c.1380G > A, p.Trp460*[c]	Nonsense mutation		Mild		
	TUBGCP5	c.2180T > G p.Phe727Cys with 15q11.2 BP1-BP2 microdeletion[d]	Missense variant		Mild	Primary microcephaly DD	No cortical malformation Normal
	TUBGCP6	c.2066-6A > G, p.Asp689Valfs*2[e] c.4485-21A > C,Cmp Het[e]	Cyriptic splice site Out-of-frame transcript truncated protein		Mild	Microcephaly ID, Rod-cone dysfunction	Mild

(*Continued on next page*)

Table 1. *Continued*

Function	Gene	Variants (nucleotide/ protein/zygosity)	Effects		Severity	Clinical features	Common MRI findings (# of positive cases/ # of total cases)
CM1 domain ɣ-TuRC targeting genes	CDK5RAP2	c.243T > A, p.Ser81X Hom[f]	Nonsense mutation	Truncated protein functional loss	Mild-moderate	Primary microcephaly (MCPH3) (Severe microcephaly) ID/MR	Simplified gyral pattern Reduced cerebral cortical volume Corpus callosum hypogenesis
		c.246T > A, p.Tyr82X Hom[g]	Nonsense mutation				
		c.IVS26-15A > G p.Glu385fs*4, Hom[f,g]	Alternative splice acceptor site and premature termination codon				
		c.700G > T, p.Glu234X Hom[h]	Premature termination codon		Mild-moderate (+SNHL, hypotonia)		
		c.4546G > T, p.Glu1516X c.4672C > T, p.Arg1558X, Cmp Het[i]	Nonsense mutation		Severe (+mixed conductive-SNHL, simplified gyria, short stature		
		c.524_528del, p.Gln175Argfs*42 c.4005-1G-A, Cmp Het[j]	Frameshift mutation, splicing defect, premature termination codon		Mild-moderate		
		c.4604+1G > C p.Val1526fs*15 c.3097delG, p.Val1033fs*41, Cmp Het[k]	Alternative splice acceptor site, premature termination codon, and frameshift mutation		Moderate (+cafe au lait lesions, facial dysmorphism)		
		c.4441C > T, p.Arg1481X Hom[l]	Nonsense mutation		Moderate (simplified gyria, CC agenesis)		

ɣ-TuSC, gamma-tubulin small complex; ɣ-TuRC, gamma-tubulin ring complex; TUBGCP-2,4,5,6, tubulin gamma complex associated protein-2,4,5,6; HAUS6, HAUS augmin-like complex subunit-6; NEDD1, neural precursor cell expressed developmentally down-regulated 1; CDK5RAP2, CDK5 regulatory subunit-associated protein 2; Hom, homozygous; Het, heterozygous; Cmp, compound; dup, duplication; del, deletion; Ala, alanine; Arg, arginine; Asp, aspartic acid; Cys: cysteine; Glu, glutamic acid; Gln, glutamine; Gly, glycine; Ile, isoleucine; Leu, leucine; Lys, lysine; Phe, phenylalanine; Pro, proline; Ser, serine; Trp, tryptophan; Tyr, tyrosine; Val, valine; DD, developmental delay; ID, intellectual delay; SNHL, sensory neural hearing loss; CC, corpus callosum; MCCRP, microcephaly and chorioretinopathy; MCPH3, primary microcephaly 3; MRI, magnetic resonance imaging.

[a]Mitani T, Punetha J, Akalin I, Pehlivan D, Dawidziuk M, Akdemir ZC, et al. Biallelic Pathogenic Variants in TUBGCP2 Cause Microcephaly and Lissencephaly Spectrum Disorders Am J Hum Genet. 2019:1–11. https://doi.org/10.1016/j.ajhg.2019.09.017.

[b]Scheidecker S, Etard C, Haren L, Stoetzel C, Hull S, Passemard S, et al. Mutations in TUBGCP4 Alter Microtubule Organization via the g -Tubulin Ring Complex in Autosomal-Recessive Microcephaly with Chorioretinopathy Am J Hum Genet. 2015 Apr 2; 96(4):666-74. https://doi.org/10.1016/j.ajhg.2015.02.011.

[c]Da Palma MM, Motta FL, Takitani GEDS, Salles MV, Lima LH, Ferraz Sallum JM. TUBGCP4 – associated microcephaly and chorioretinopathy Ophthalmic Genet. 2020 Apr; 41(2):189-193. https://doi.org/10.1080/13816810.2020.1747084.

[d]Maver A, Čuturilo G, Kovanda A, Miletić A, Peterlin B. Rare missense TUBGCP5 gene variant in a patient with primary microcephaly Eur J Med Genet. 2019 Dec; 62(12):103598. https://doi.org/10.1016/j.ejmg.2018.12.003.

[e]Hull S, Arno G, Ostergaard PIA, Pontikos N, Robson AG, Webster AR, et al. Clinical and Molecular Characterization of Familial Exudative Vitreoretinopathy Associated With Microcephaly Am J Ophthalmol. 2019 Nov; 207:87-98. https://doi.org/10.1016/j.ajo.2019.05.001.
[f]Bond J, Roberts E, Springell K, Lizarraga S, Scott S, Higgins J, et al. A centrosomal mechanism involving CDK5RAP2 and CENPJ controls brain size Nat Genet. 2005 Apr; 37(4):353-5. https://doi.org/10.1038/ng1539.
[g]Hassan MJ, Khurshid M, Azeem Z, John P, Ali G, Chishti MS, et al. Previously described sequence variant in CDK5RAP2 gene in a Pakistani family with autosomal recessive primary microcephaly BMC Med Genet. 2007 Sep 1; 8:58. https://doi.org/10.1186/1471-2350-8-58.
[h]Pagnamenta AT, Murray JE, Yoon G, Akha ES, Harrison V, Bicknell LS, et al. A Novel Nonsense CDK5RAP2 Mutation in a Somali Child With Primary Microcephaly and Sensorineural Hearing Loss Am J Med Genet A. 2012 Oct; 158A(10):2577-82. https://doi.org/10.1002/ajmg.a.35558.
[i]Lancaster MA, Renner M, Martin C, Wenzel D, Bicknell LS, Hurles ME, et al. Cerebral organoids model human brain development and microcephaly. Nature 2013; 501:373–9. https://doi.org/10.1038/nature12517.
[j]Tan CA, Topper S, Ward C, Stein J, Reeder A, Arndt K, et al. The first case of CDK5RAP2 -related primary microcephaly in a non-consanguineous patient identified by next generation sequencing. Brain Dev 2014; 36:351–5. https://doi.org/10.1016/j.braindev.2013.05.001.
[k]Pagnamenta AT, Howard MF, Knight SJL, Keays DA, Quaghebeur G, Taylor JC, et al. Activation of an exonic splice-donor site in exon 30 of CDK5RAP2 in a patient with severe microcephaly and pigmentary abnormalities Clin Case Rep. 2016 Aug 23; 4(10):952-956. https://doi.org/10.1002/ccr3.663.
[l]Issa L, Mueller K, Seufert K, Kraemer N, Rosenkotter H, Ninnemann O, et al. Clinical and cellular features in patients with primary autosomal recessive microcephaly and a novel CDK5RAP2 mutation. Orphanet J Rare Dis. 2013 Apr 15; 8:59. https://doi.org/10.1186/1750-1172-8-59).

Table 2. Summary of the clinical presentation of patients with *TUBGCP2* mutations.

Case Gender Age	Origin/ consanguinity/ gestation	Lissencephaly	Microcephaly	Developmental delay	Seizure-epilepsy onset/type	Other clinical features	Neurological examination	Physcomotor involvement	Brain MRI	Variant nucleotide/ protein
Patient 1 Female 10 yo This paper	Turkish Yes Term	+	++	+	Intractable epilepsy 6 mo	Narrow forehead, thick eyebrows, prominent ear, bulbous nose, separated teeth, retrognathia	Hypotonia, muscle atrophy, contractures, spasticity, brisk DTRs	Loss of all motor and cognitive skills	10 y: Pachygyria, cerebral and cerebellar atrophy, cystic foci in white matter, and thinning of the corpus callosum	c.1015G > A p.Glu311Lys Homozygous
Patient 2 Male 6 yo This paper	Turkish Yes Term	+	++	+	Intractable epilepsy 3 yo	NA	Contractures, spasticity, increased DTRs	Prominent at 2 yo/walks with assistance	6 y: Pachygyria, cerebral and cerebellar atrophy, decreased white matter volumes, cystic foci at the centrum semiovale and thin corpus callosum	c.1015G > A p.Glu311Lys Homozygous
Family 1 Case 1 Male 6 yo [1]	Turkish Yes Term	+	+	+	Generalized seizures 6 y 9 mo	Narrow forehead, upslanting palpebral fissures, bulbous nose, prominent ear, widely spaced teeth, thick eyebrows, smooth philtrum, thin upper lip, pectus excavatum	Truncal hypotonia, normal DTRs, myopia	Delayed motor and language skills, autistic features	21 m: Pachygyria, thin corpus callosum, especially in the posterior region, mild cerebellar atrophy	c.997C > T p.Arg333Cys Homozygous *de novo* 2q23.1 dup (MBD5)
Family 1 Case 2 Male 7 yo [1]	Turkish Yes Term	+	+	+	No seizure	Narrow forehead, bulbous nose, prominent ear, smooth philtrum, retrognathia	Normal tone, normal DTRs	Normal motor skills, difficulty in reading	6 m: Posterior dominant pachygyria	c.997C > T p.Arg333Cys Homozygous
Family 2 Female 1yo 3mo [1]	Indian No Preterm (31 weeks)	+	+	+	Generalized seizures 5mo	Short and sloped forehead, thick eyebrows, puffy eyelids, full lips, retromicrognathia Exitus at ≅3 yo	Truncal hypotonia, brisk DTRs, spasticity, cortical blindness	Severely delayed motor and language skills	5 m: Pachygyria loss of white matter, thinning of the corpus callosum, volume loss of pons, and exuberant subependymal cyst formation, subependymal heterotipia, subcortical band	c.1843G > C p.Ala615Pro Homozygous
Family 3 Male 4 yo [1]	Iranian Yes Preterm (27 weeks)	+	+	+	Generalized seizures 7 mo	Bitemporal narrowing, upslanting palpebral fissure, micrognathia, midface hypoplasia, prominent ears and lips	Truncal hypotonia, no spasticity, optic atrophy, retinal changes	Severely delayed motor and language skills	1 year: Pachygyria, hyperintense periventricular white matter, very thin corpus callosum, and subependymal cysts, subcortical band, thin pons	c.1843G > C p.Ala615Pro Homozygous
Family 4 Male 8 yo [1]	Polish No Term	+	+	+	Generalized seizures	Smooth philtrum, prominent ears	Normal DTRs, no spasticity, myopia, astigmatism	Delayed motor and language skills	8 y: Pachygyria in the temporal lobes and partial thinning of the corpus callosum	c.889C > T p.Arg297Cys c.2025-2A > G Com Het

MRI, magnetic resonance imaging; yo, years old; mo, months; DTR, deep tendon reflexes.

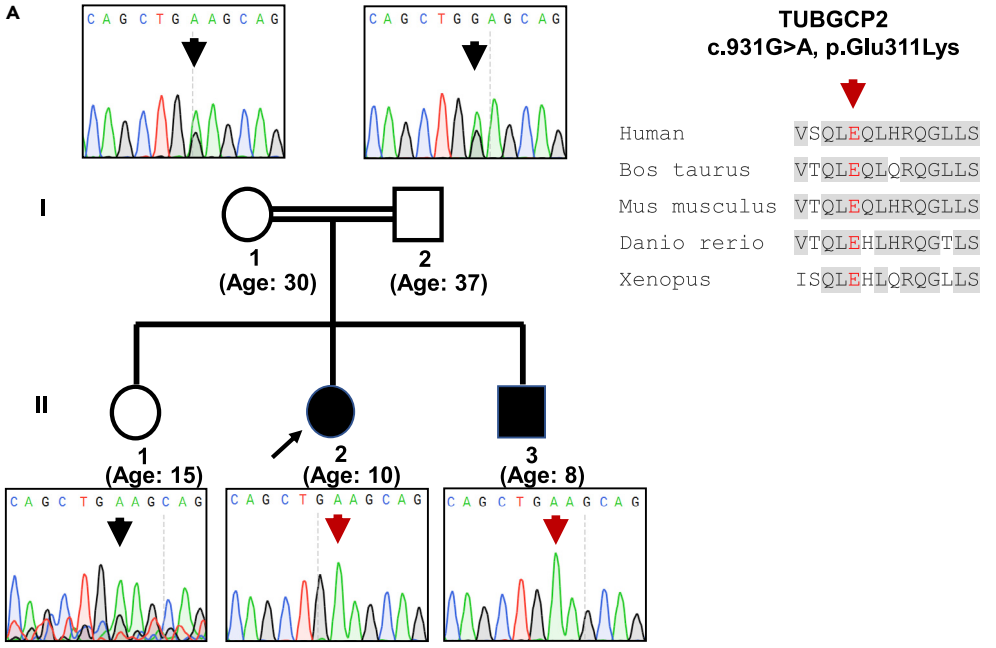
A
C A G C T G A A G C A G
C A G C T G G A G C A G
TUBGCP2
c.931G>A, p.Glu311Lys
Human VSQLEQLHRQGLLS
Bos taurus VTQLEQLQRQGLLS
Mus musculus VTQLEQLHRQGLLS
Danio rerio VTQLEHLHRQGTLS
Xenopus ISQLEHLQRQGLLS
I
1
(Age: 30)
2
(Age: 37)
II
1
(Age: 15)
2
(Age: 10)
3
(Age: 8)

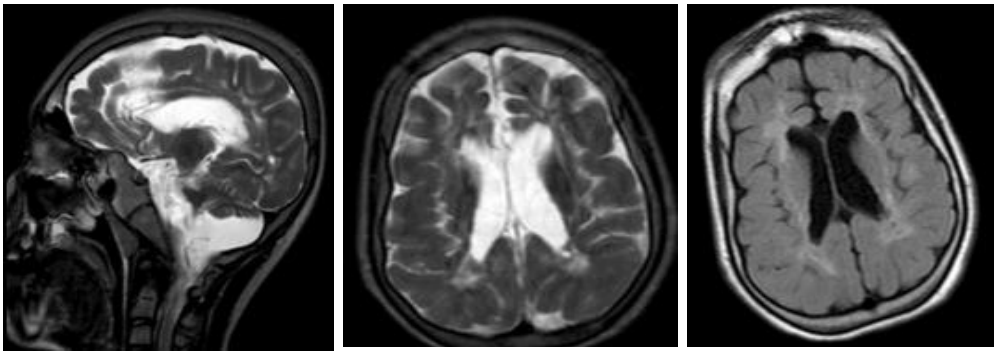
B

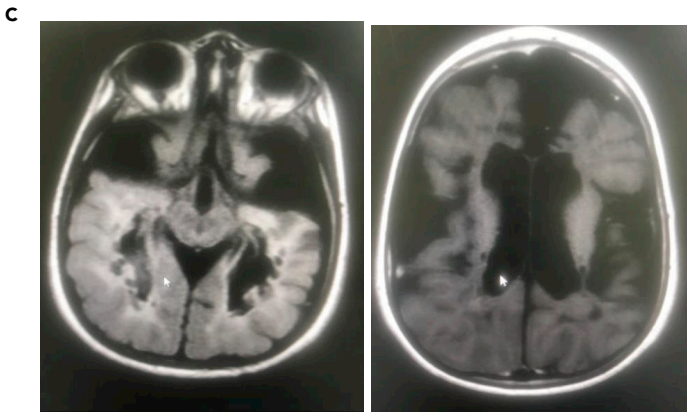
C

Figure 1. Clinical presentation and brain MRI of the patients

(A) Pedigree and sequence data including the conservation of the protein.

(B) Cranial T2-weighted MR images of the index patient showed pachygyria, cerebellar parenchymal atrophy, bilateral volume loss in cerebral white matter, cystic foci with increased intensity in the neighboring white matter, and thinning of the corpus callosum.

(C) Her affected sibling's MRI detected cerebral and cerebellar atrophy and cystic foci with decreased white matter volumes.

corpus callosum (Figure 1B). Her 8-year-old brother demonstrated normal developmental milestones until 8 months of age, when developmental delay was noticed and became evident after 2 years of age. Intractable seizures started after 3 years of age. His neurological examination at 8 years of age revealed microcephaly, atrophy and contractures of the extremities, increased deep tendon reflexes, and spasticity. He was able to walk with assistance. Cranial MR detected cerebral and cerebellar parenchymal atrophy, significantly decreased white matter volumes, cystic foci with neighboring hyperintensities at the centrum semiovale and thin corpus callosum (Figure 1C and Table 2).

Genetic analysis by whole exome sequencing

We performed whole exome sequencing (WES) in both siblings and their parents as described previously (Balaraju et al., 2020). We identified a homozygous variant in *TUBGCP2* exon 8 (NP_006650.1: c.931G > A, p.Glu311Lys, hg19 chr10:135106636) within the extended Grip1 domain in both siblings, while both parents and a 15-year-old healthy sibling are heterozygous carriers (Figure 1A). This variant has not been reported previously and not present in gnomAD or in a cohort of 1,182 ethnically matched Turkish control individuals (TUBITAK MAM-GMBE data set: http://gmbe.mam.tubitak.gov.tr/en). *In silico* analysis suggested that c.931G > A, p.Glu311Lys is deleterious, using prediction tools such as Polyphen2 (http://genetics.bwh.harvard.edu/pph2/), CADD (https://cadd.gs.washington.edu/), and SIFT (http://sift.jcvi.org/) to assess pathogenicity. Sanger sequencing confirmed that this variant is homozygous in the patients and heterozygous in the healthy parents.

Analysis of components of γ-TuRC

As TUBGCP2 is a core component of the γ-TuRC nucleation complex, we studied the localization of some γ-TuRC components and associated proteins in control and *TUBGCP2* mutated human fibroblasts in interphase and in mitosis by immunofluorescence, as well as the levels of the GCP2 protein along the cell cycle (Figure 2). We observed a faint delocalization of γ-tubulin in the mitotic cells of the patient fibroblasts. This suggested that the mutation in TUBGCP2 could perturb γ-TuRC localization pattern. To test this hypothesis, we looked at the localization of other components of the γ-TuRC complex such as HAUS augmin-like complex subunit 6 (HAUS6), protein NEDD1 (NEDD1), and pericentrin (PCNT), an integral component of the PCM of the centrosome involved in the initial establishment of organized MT arrays in mitosis (Figure 3A). We did not detect any significant changes in the patient fibroblasts in interphase (Figure 3A upper panel). However, in mitosis, patient fibroblasts presented a faint delocalization of two components associated with the γ-TuRC complex, HAUS6 and NEDD1 (Figure 3A, lower panel, and 3C). The localization of HAUS6 was clearly affected at all stages of mitosis as the protein presents with a diffuse pattern throughout the cytoplasm (Figure 3A). In contrast, there was no visible effect on the centrisomal localization of PCNT neither in interphase nor in mitosis.

Next, we wondered whether the levels of TUBGCP2 in the patient fibroblast could be altered and, in turn, affect the localization of other γ-TuRC components or associated proteins. To test this hypothesis, we synchronized control and patient fibroblasts and checked the levels of TUBGCP2 (Figure 3B). As synchronization and loading controls, we used acetylated tubulin (increased in G_0) and TPX2 (increased in mitosis). We did not observe any significant change in the levels of TUBGCP2 in control and patient fibroblasts along the cell cycle. Acetylated tubulin was increased in G_0 and TPX2 in mitosis, confirming a correct synchronization of cells.

Structural modeling of the *TUPBGCP2* missense mutation

GCP2:CGP3 inter-molecular interactions make up nearly half of the γ-TuRC ring complex (Wieczorek et al., 2020) (Figure 3C). The E311 of GCP2 is located across the interaction core of each asymmetric GCP2:GCP3 complex with 3,000 A 2 interface between GCP2 and GCP3 within the complex. The acidic nature of E311 is complemented by the surrounding basic residues of GCP2 (R315) and GCP3 (R365 and R366 of GCP3). The

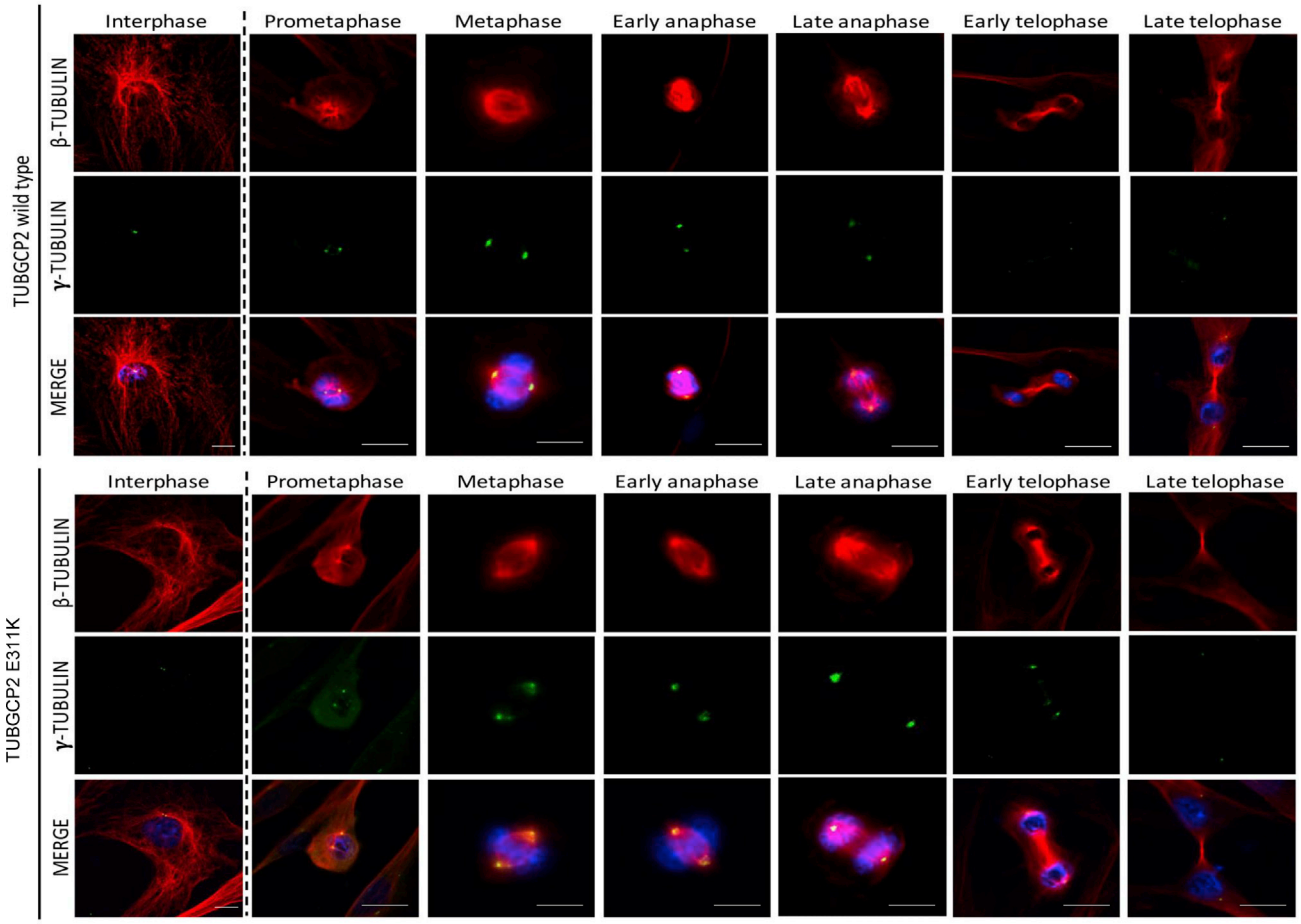

Figure 2. γ-Tubulin localization is affected in TUBGCP2 p.Glu311Lys (E311K) fibroblasts

Asynchronous cells were stained for γ-tubulin (green), β-tubulin (red), and DNA (blue), and different phases of mitosis were captured. Scale bar, 10 μm.

E311K mutation of GCP2 induces a disruption in this complementarity. This is highlighted with the mutation-induced change in the electrostatic surface of GCP2, facing to GCP3 (Figure 4). As a result, the rather acidic GCP2 patch gets modified into a basic one, which would be repelled by the basic GCP3 surface.

Proteomics studies with label-free liquid chromatography mass-spectrometry

We applied proteomics to study the functional effect of the *TUBGCP2* mutation in fibroblasts. Proteomics allows the unbiased discovery of pathophysiological processes in rare neurodegenerative and neuromuscular diseases (Roos et al., 2018), and based on previous studies, fibroblasts were proven to represent a suitable model to study the molecular etiology of neurological diseases (Mingirulli et al., 2020) (Hentschel et al., submitted to this issue). Therefore, we analyzed a human skin fibroblast protein library for the expression of TUBGCP2 and identified 14 unique peptides covering 23% of the entire protein (Figure S2). This result demonstrates the expression of TUBGCP2 in human fibroblasts and thus indicates the suitability of these cells to study the effect of TUBGCP2 mutations *in vitro*. Moreover, expression data of TUBGCP2 (https://gtexportal.org/home/gene/TUBGCP2) show that this protein is highly expressed in fibroblasts and skin, in similar levels with the brain cerebellum which has one of the highest expression levels of *TUBGCP2* (Figure S1) reinforcing the suitability of this cellular model.

Next, we applied a label-free liquid chromatography mass-spectrometry (LC-MS/MS) approach to investigate the proteomic signature of human skin fibroblasts derived from the index patient with the homozygous *TUBGCP2* c.931G > A, p.Glu311Lys mutation. This unbiased study revealed a statistically significant (p-ANOVA $\leq$ 0.05) dysregulation of 50 proteins: 26 were increased and 24 decreased (Table S1; $\leq$0.46 =

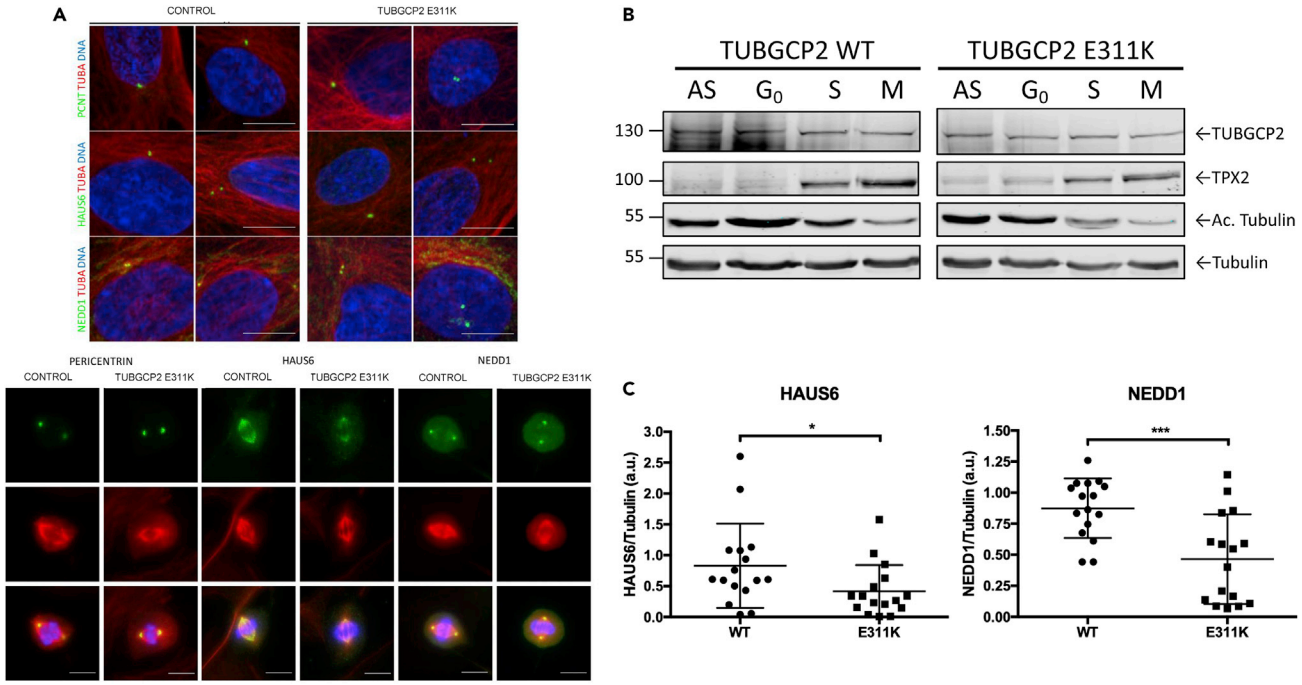

Figure 3. Similar TUBGCP2 levels are present in control and patient fibroblasts along the cell cycle

(A) Asynchronous cells were stained for either PCNT, HAUS6 or NEDD1 (green), α- or β-tubulin (red), and DNA (blue), and interphase cells (upper panel) or different phases of mitosis (lower panel) were captured. Immunofluorescence images of wild-type and *TUBGCP2* mutant (p.Glu311Lys) fibroblasts in metaphase showing that the localizations of HAUS6 and NEDD1 are altered in the mutant cells. Scale bar, 10 μm.

(B) Similar TUBGCP2 levels are present in control and patient fibroblasts along the cell cycle. Cells were synchronized in G_0 (48 hr of serum starvation), S phase (double thymidine block), and mitosis (double thymidine/nocodazole block), and 50 μg of total cell lysate was loaded onto 10% SDS-PAGE. Antibodies used in this Western blot were as follows: rabbit a-TPX2 (1 ug/ml), rabbit anti-TUBGCP2 (1:2000), mouse anti-AcTubulin (1:1000), and rabbit anti-tubulin (1:500). Scale bar, 10 μm.

(C) The signal intensity of HAUS6 and NEDD1 was quantified and normalized to either the α- or β-tubulin signal intensity depending on the combination of antibodies used. Fifteen metaphases have been analyzed for each condition and represented in scatted plots. Data are represented as mean ± SEM. *P < 0,05 and ***P < 0.001, Student's t-test).

significantly decreased and ≥2.24 = significantly increased). Further *in silico*-based pathway analyses (proteomaps based on the "Kyoto Encyclopedia of Genes and Genomes" [KEGG]; [Liebermeister et al., 2014]) of these proteins suggested that proteins involved in the assembly and organization of the cytoskeleton and the extracellular matrix are affected along with proteins controlling cellular adhesion. In addition, our proteomic findings raise the possibility that *TUBGCP2* mutations affect other cellular processes such as different metabolic (glycolysis, lipid and sterol oxidation, and amino acid metabolism) and signaling (MAPK, PI3K-AKT, and WNT) pathways (Figure 5A). Results of a gene ontology-based analysis of our proteomic data revealed that proteins crucial for neuronal homeostasis including axon guidance are also affected (Figures 5B and 5C and Table S1). Further analysis of functional protein association networks via STRING (and Cytoscape [Shannon et al., 2003]) indicated a potential functional interplay of several proteins affected by mutant TUBGCP2 (Figure 5D). In addition, we analyzed the abundance of 8 tubulins identified in our comparative proteomic profiling approach regardless of the above mentioned cut-off values for up- or down-regulation. One (tubulin beta-3 chain) shows an increase of more than 25%, whereas three (tubulin beta chain, tubulin beta-4B chain, and tubulin alpha-1C chain) presented with more than 25% decrease in abundance (Figure 5D) indicating an effect of *TUBGCP2* mutations on other tubulin proteins.

Immunofluorescence studies on human skin fibroblasts confirm proteomic findings

Immunofluorescence studies on TUBGCP2-patient-derived and control fibroblasts were carried out to validate our proteomic findings. In line with our mass spectrometric based protein quantification, immunological investigation of αB-crystallin (CRYAB) revealed increased abundance with focal cytoplasmic accumulations (white arrows) in patient-derived cells (Figure 6A). Studies of D-3-phosphoglycerate dehydrogenase

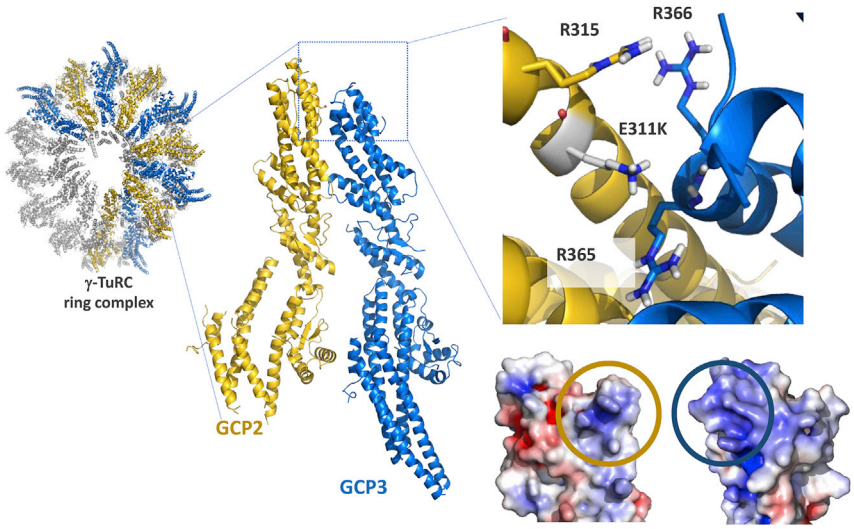

Figure 4. Computational modeling of the E311K mutation

The γ-TuRC ring complex contains five repeating units of GCP2 (gold cartoon) and GCP3 (marine cartoon) complex (pdb id: 6v6s). The acidic GCP2-E311 is complemented by the basic environment made of three arginine residues (R315 of GCP2, R365, and R366 of GPC3). The indicated charge complementarity will be lost upon E311K mutation. This is depicted by the mutation-induced change in the electrostatic distribution of GCP2, facing GCP3. The interacting surfaces of GCP2 and GCP3 are encircled in gold and marine, respectively.

(PHGDH) and tenascin confirmed the reduced abundances of both proteins as identified by proteomic profiling (Figure 6A). Prompted by the identified increase of lysosome membrane protein 2 (Figure 5) indicative for increased activation of a lysosomal protein degradation pathway, we investigated levels of CD63, a member of the tetraspanin superfamily commonly used as a marker of late endosomes and lysosome-related organelles. Compared to control cells, fibroblasts derived from the TUBGCP2-patient presented with a profound increase of CD63 immunoreactivity (Figure 6A). In accordance with our proteomic findings, immunofluorescence studies of desmin (DES) revealed an increased level of this type III intermediate filament in the TUBGCP2-patient-derived fibroblasts (Figure 6A). Prompted by the general vulnerability of cytoskeletal and cytoskeleton remodeling proteins in patient-derived cells including increase of adseverin, a Ca^{2+}-dependent actin filament-severing protein, we investigated F-actin level and distribution by FITC-phalloidin staining. Results of these studies revealed increase of thicker actin bundles (Figure 6A) most likely referring to actin stress fibers in patient cells.

L-serine supplementation reduces cytotoxicity in TUBGCP2-patient-derived fibroblasts

Proteomic profiling identified PHGDH as a protein significantly altered in abundance in the *in vitro* model of TUBGCP2. Given that recessive PHGDH mutations also result in a neurological phenotype and that PHGDH-patients respond to L-serine treatment, the effect of L-serine treatment was pre-clinically addressed in cultured skin fibroblasts derived from the TUBGCP2-patient: although investigation of the proliferation revealed an increase of 8% in fibroblasts of both, TUBGCP2-patient and control upon L-serine supplementation, in patient-derived cells, a 26% reduction of cytotoxicity was detected compared to 14% in control cells (Figure 6B).

Discussion

MTs are long fibers made of 13 protofilaments of α- and β-tubulin heterodimers (Wu and Akhmanova, 2017). Considered as one of the main cytoskeleton elements, they are involved in intracellular transport, organelle positioning, motility, signaling, and cell division (Kollman et al., 2010). MTs are nucleated at the MT organizing centers, most importantly the centrosome, which is an organelle composed of 2 perpendicular barrels of 9 triplets of MTs surrounded by the pericentriolar material (Teixido-Travesa et al., 2012). The levels of TUBGCP2 were comparable in control and patient fibroblasts suggesting that the stability of the mutated protein along the cell cycle is not affected. In fibroblasts of the patient, the protein steady state level of TUBGCP2 was not significantly altered. However, in mitosis, patient fibroblasts presented a faint

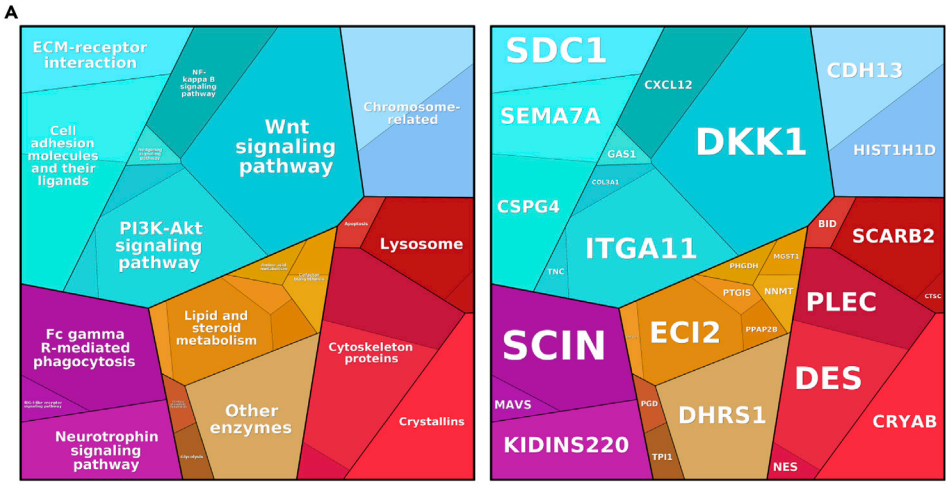
A
ECM-receptor interaction
Cell adhesion molecules and their ligands
Wnt signaling pathway
Chromosome-related
PI3K-Akt signaling pathway
Lysosome
Fc gamma R-mediated phagocytosis
Lipid and steroid metabolism
Cytoskeleton proteins
Other enzymes
Crystallins
Neurotrophin signaling pathway
SDC1
CXCL12
CDH13
SEMA7A
DKK1
HIST1H1D
GAS1
CSPG4
ITGA11
BID
SCARB2
PLEC
SCIN
ECI2
DES
MAVS
DHRS1
CRYAB
KIDINS220
NES

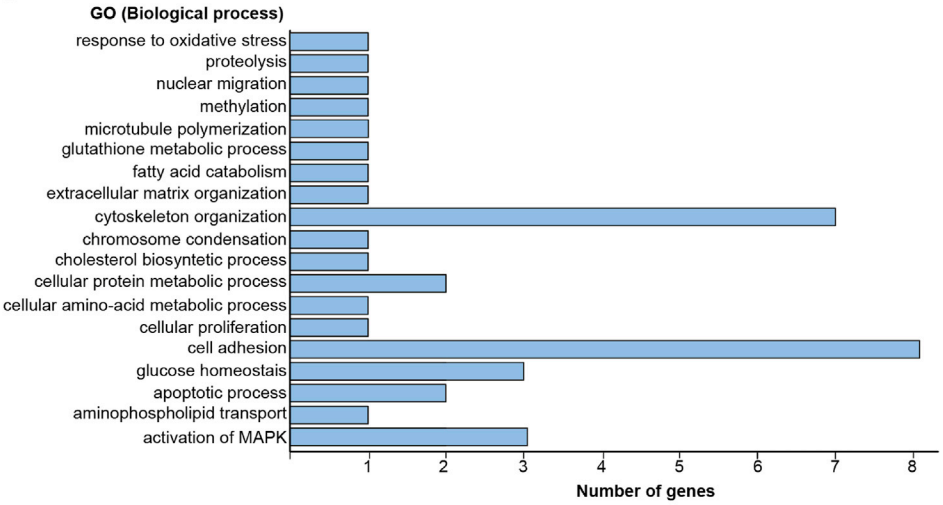
B
GO (Biological process)
response to oxidative stress
proteolysis
nuclear migration
methylation
microtubule polymerization
glutathione metabolic process
fatty acid catabolism
extracellular matrix organization
cytoskeleton organization
chromosome condensation
cholesterol biosyntetic process
cellular protein metabolic process
cellular amino-acid metabolic process
cellular proliferation
cell adhesion
glucose homeostais
apoptotic process
aminophospholipid transport
activation of MAPK
1
2
3
4
5
6
7
8
Number of genes

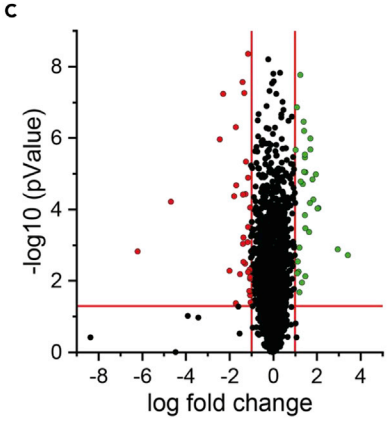
C
-log10 (pValue)
8
6
4
2
0
-8
-6
-4
-2
0
2
4
log fold change

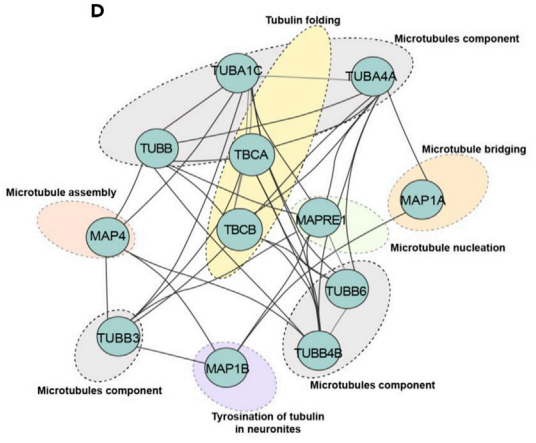
D
Tubulin folding
Microtubules component
TUBA1C
TUBA4A
TUBB
TBCA
Microtubule bridging
Microtubule assembly
MAP1A
MAP4
TBCB
MAPRE1
Microtubule nucleation
TUBB6
TUBB3
TUBB4B
MAP1B
Microtubules component
Microtubules component
Tyrosination of tubulin in neuronites

Figure 5. Proteomics analysis of TUBGCP2 and control fibroblasts

(A) Proteomap resulting from the comparative proteome profiling of TUBGCP2 fibroblasts versus control cells. Every polygon or circle represents a protein, the size of which is given by the fold change. The proteins are then grouped in functional categories based on the KEGG database. The proteomap shows five main hierarchy levels, which are further divided into sub-pathways.

(B) In silico analysis of dysregulated proteins utilizing GO term (biological pathway) annotation showing that proteins involved in cell adhesion and cytoskeleton organization are majorly affected by the TUBGCP mutation.

(C) Volcano plot shows proteins which are significantly increased or decreased, compared to control fibroblasts.

(D) String analysis visualized using Cytoscape of microtubule and microtubule-associated proteins identified within our proteomic analysis.

delocalization of two components associated with the γ-TuRC complex (HAUS6 and NEDD1, Figure 3). Expanding on our structural analysis, we propose that this mutation impacts the stability of the γ-TuRC ring potentially caused by the charge swap introduced by the c.931G > A, p.Glu311Lys variant, which is predicted to change the electrostatic complementarity of the GCP2:GCP3 interface. The c.931G > A, p.Glu311Lys mutation seen in our patient is situated between the two Grip1 domain variants previously reported, namely c.889C > T (p.Arg297Cys) and c.997C > T (p.Arg333Cys). Our data suggest that in contrast to as hypothesized by Mitani et al. (Mitani et al., 2019), mutations in the Grip1 domain may affect the localization of γ-TuRC and the mutation does not impinge on the steady-state level of the GCP2 protein (Figure 3).

Results of our proteomic profiling revealed the altered abundance of a total of 50 proteins suggesting a cellular vulnerability against homozygous *TUBGCP2* missense mutations. Interestingly, other tubulin proteins are affected only to a minor degree (Figure 5). The cytoskeleton appears to be affected by the expression of mutant TUBGCP2, as several proteins crucial for the assembly and maintenance of cellular cytoskeleton such as DES, plectin, adseverin, PDZ and LIM domain protein 5, syndecan, nestin, and EH domain-binding protein 1 are dysregulated. Notably, some of those cytoskeletal proteins are known to be involved in neuronal functions: Nestin overexpression has been shown to be crucial for brain development by regulating cell proliferation and neuronal progenitor cell division; it is used as a marker of neuronal progenitor cells (Liu et al., 2015). Syndecan-1 regulates the maintenance and proliferation of neural progenitor cells during mammalian cortical development, which has potential relevance for the prominent neuronal migration defects seen in the patients (Wang et al., 2012).

Pathogenic amino acid substitutions in TUBGCP2 may also lead to dysregulation of proteins involved in cellular adhesion to the extracellular matric (ECM), an important process for cell migration and invasion. Both processes are tightly associated with the MT network (Seetharaman and Etienne-Manneville, 2019) (Figure 5). For example, integrin signaling plays a crucial role in cell adhesion by altering MT stabilization, organization, and dynamics. Of note, our data suggest altered expression of integrin alpha-11, semaphorin 7A (Pasterkamp et al., 2003), and matrix-remodeling-associated protein 8 (Jung et al., 2012) (Table S1) supporting the concept of a possible perturbed integrin signaling in TUBGCP2-patient-derived cells. Moreover, numerous studies of initial myelination and remyelination stages in the central nervous system demonstrated the importance of a functional interplay between several key cytoskeletal components and integrin superfamily proteins, which is in line with the white matter abnormalities detected in our patients (e.g. [Miyata, 2019]).

Interestingly, *TUBGCP2* mutations may also affect metabolic processes, some of which are of great importance in neuronal cells (Figure 5): PHGDH, the first step enzyme in the *de novo* production of L-serine, an amino acid crucial for brain development and neuron survival (Hirabayashi and Furuya, 2008) was found to be decreased in patient-derived *TUBGCP2*-mutant fibroblasts. Several publications highlighted the importance of L-serine in central nervous system (CNS) development and maintenance, and supplementation with L-serine was found to have a beneficial effect in motor neuron disease (Levine et al., 2017) linked to neuroprotection through the modulation of the endoplasmic reticulum (ER) stress response (Dunlop et al., 2018) and in hereditary sensory and autonomic neuropathy due to mutations in *SPTLC1* (Fridman et al., 2019).

Of note, PHGDH deficiency was linked to a neurological disease defined by congenital microcephaly, psychomotor retardation, and seizures, as well as neuropathy (Jaeken et al., 1996; Poli et al., 2017). Prompted by the neurological phenotype observed in our patients and the above mentioned impact of L-serine

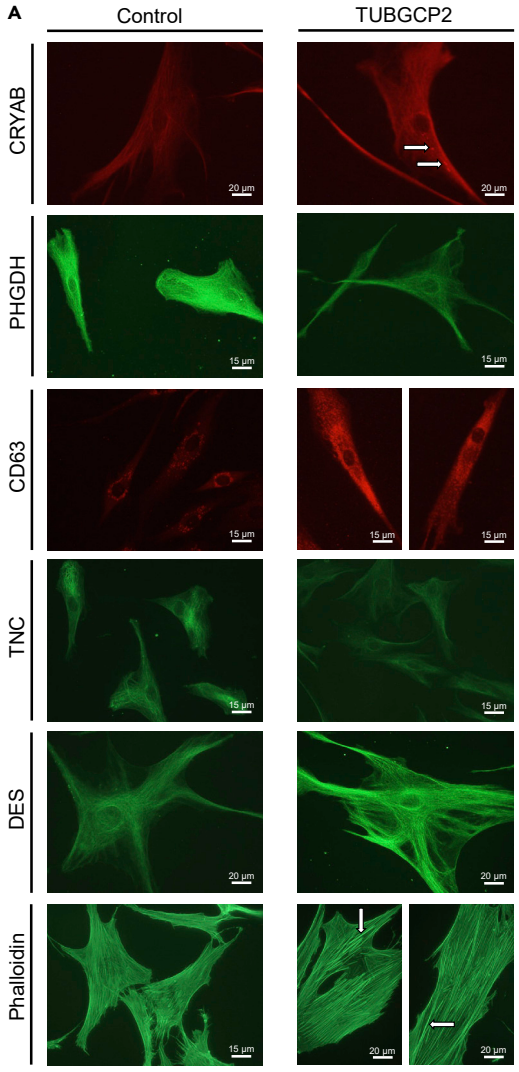
A
Control
TUBGCP2
CRYAB
PHGDH
CD63
TNC
DES
Phalloidin
20 µm
15 µm

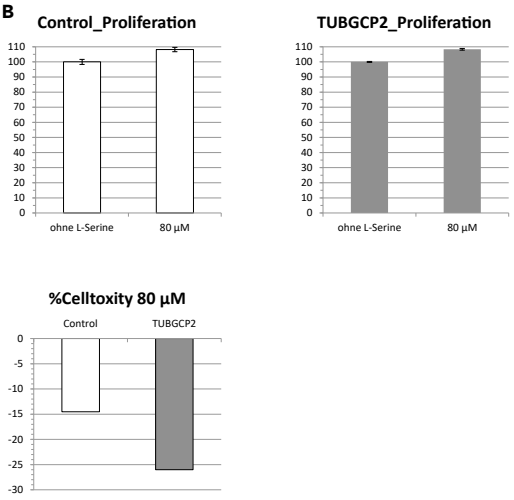
B
Control_Proliferation
TUBGCP2_Proliferation
110
100
90
80
70
60
50
40
30
20
10
0
ohne L-Serine
80 µM
%Celltoxity 80 µM
Control
TUBGCP2
0
-5
-10
-15
-20
-25
-30

Figure 6. Immunohistochemical studies confirmed proteomics findings in patient fibroblasts

(A) Immunofluorescence studies on TUBGCP2-patient-derived fibroblasts detected increased abundance of αB-crystallin (CRYAB) (white arrows), CD63, desmin, and phalloidin, while reduced levels of D-3-phosphoglycerate dehydrogenase (PHGDH) and tenascin (TNC), confirming the findings detected by proteomics analysis. Scale bar is shown on each image. (B) L-serine treatment in cultured skin fibroblasts revealed an 8% increased proliferation in both TUBGCP2-patient and control, while a 26% reduction of cytotoxicity was detected in patient-derived cells compared to 14% in controls. These changes did not reach statistical significance. Data are represented as mean ± SEM.

produced by PHGDH on neuronal function and survival, we preclinically tested the effect of L-serine supplementation on fitness of patient-derived fibroblasts. Results of these studies demonstrated a beneficial effect of L-serine treatment in fibroblasts, a valuable model to study the molecular etiology of neurological diseases (Hentschel et al., preprint available https://doi.org/10.21203/rs.3.rs-48014/v1), thus suggesting that L-serine treatment might represent a concept to ameliorate the phenotype.

Although MT polymerization has been claimed to have an impact on several metabolic processes, such as glycolysis (Cassimeris et al., 2012), we could observe indeed a decrease of proteins involved in glycolysis (triosephosphate isomerase), gluconeogenesis (6-phosphogluconate dehydrogenase), and glucose homeostasis (insulin-like growth factor-binding protein 5) in TUBGCP2-deficient fibroblasts. These processes are crucial for proper brain functioning, and their dysregulation has already been linked to the manifestation of neurological diseases (Mergenthaler et al., 2013).

Proteomic profiling also suggested that proteins involved in the activation of MAPK may be up-regulated in the patient-derived cells and might be involved in the molecular etiology of the disease: Kinase D-interacting substrate of 220 kDa is a multifunctional scaffold protein involved in neuronal development, neurite outgrowth, and maturation (Scholz-Starke and Cesca, 2016) and its increase in TUBGCP2-patient-derived fibroblasts might reflect a possible rescue mechanism. In contrast, an increase in chondroitin sulfate proteoglycan 4, as identified in patient-derived fibroblasts, may be associated with the inhibition of functional recovery by impeding axonal sprouting and synaptic rearrangements as suggested previously (Loers et al., 2019).

Several proteins dysregulated upon the homozygous *TUBGCP2* missense mutation play crucial roles in the development and maintenance of the nervous system, highlighting that axon and neurite outgrowth/elongation may be affected along with perturbed neuronal differentiation, migration, and synaptic plasticity. Hence, our proteomic findings obtained in primary patient fibroblasts hint toward possible pathophysiological downstream effects of *TUBGCP2* mutations on normal development and functioning of the nervous system and thus provide insight for the clinical manifestation of *TUBGCP2*-associated neuropediatric disease. Moreover, human skin fibroblasts show promise to further delineate the pathophysiology and explore potential treatments for this rare disorder.

In summary, we describe two siblings carrying a homozygous *TUBGCP2* variant with a severe phenotype, and show, that in addition to a neuronal migration defect, brainstem atrophy and disturbed myelination may also be associated with *TUBGCP2* mutations, explaining the variable clinical and imaging findings.

Limitations of the study

In this study, we used human primary fibroblasts of a patient with pathogenic mutations to reveal molecular insights into the pathomechanism of a severe childhood-onset neurological disease. Fibroblasts may not be the best cell type representing neuronal cells. However, the mutant protein is expressed in fibroblasts, and we believe that our results provide relevant information on the effect of the mutant protein also in other cells types, such as the neurons, neural progenitor cells, etc. Using fibroblasts and not neuronal cells for functional studies may be a limitation of the model.

Resource availability

Lead contact

The main point of contact for responding to material and resource requests is Dr. Rita Horvath (Department of Clinical Neurosciences, University of Cambridge).

We are happy to reply to requests regarding Materials, Data and Code in this publication.

Material availability

All the materials, data generated or analyzed during this study are included in this article or in the supplemental Transparent methods and are available from the corresponding author upon request.

Data and code availability

All genetic data have been deposited in the EGA database and in RD-CONNECT under the following ID numbers: patient 1: E497133, patient 2: E477343, mother: E615258, father: E739679, unaffected sibling: E191145. These data can be made available after an authentication process.

Methods

All methods can be found in the accompanying Transparent Methods supplemental file.

Supplemental information

Supplemental Information can be found online at https://doi.org/10.1016/j.isci.2020.101948.

Acknowledgments

This study was supported by the Turkish Scientific and Research Council (TÜBITAK) research grant 216S771. Y.O. is supported by Turkish Academy of Sciences Young Investigator Programme (TUBA-GEBIP). R.H. is a Wellcome Trust Investigator (109915/Z/15/Z), who receives support from the Wellcome Centre for Mitochondrial Research (203105/Z/16/Z), Medical Research Council (UK) (MR/N025431/1), the European Research Council (309548), the Wellcome Trust Pathfinder Scheme (201064/Z/16/Z), the Newton Fund (UK/Turkey, MR/N027302/1), Evelyn Trust and Lily Foundation. A.R. received financial support by the French Muscular Dystrophy Association (AFM-Téléthon; grant 21466). The Ministerium für Innovation, Wissenschaft und Forschung des Landes Nordrhein-Westfalen, the Senatsverwaltung für Wirtschaft, Technologie und Forschung des Landes Berlin and the Bundesministerium für Bildung und Forschung is gratefully acknowledged. Sequence analysis was provided by the Broad Institute of MIT and Harvard Center for Mendelian Genomics and was funded by the National Human Genome Research Institute (UM1 HG008900 and R01 HG009141) with supplemental funding provided by the National Heart, Lung, and Blood Institute under the Trans-Omics for Precision Medicine (TOPMed) program and the National Eye Institute. I.V. and Á.A.I. were supported by the CRG internal funds, grant 2017 SGR 478 from AGAUR and grant PGC2018-096976-B-I00 from the Spanish ministry of science, innovation and universities. H.L. receives support from the Canadian Institutes of Health Research (Foundation Grant FDN-167281), the Canadian Institutes of Health Research and Muscular Dystrophy Canada (Network Catalyst Grant for NMD4C), the Canada Foundation for Innovation (CFI-JELF 38412), and the Canada Research Chairs program (Canada Research Chair in Neuromuscular Genomics and Health, 950-232279). Data were analyzed using the RD-Connect Genome-Phenome Analysis Platform developed under FP7/2007-2013 funded project (grant agreement no 305444) and funding from European Joint Programme in Rare Disease (EJP-RD) and INB/ELIXIR-ES.

Authors contribution

S.G., S.H., and I.K. participated in clinical examination, data collection, and in drafting of the manuscript. A.Y., U.Y., and N.S. participated in data collection. Y.O., Á.A.I., E.S., B.E., M.A., S.B., A.T., and D.G.M.A. participated in the genetic analysis. S.L. and S.B. were involved in the bioinformatics analysis. Á.A.I. and I.V. performed the functional studies in cells. E.K. did the high-resolution structural modeling. D.H. and A.R. performed the proteomic analysis; H.L. and R.H. were responsible for the study design, data collection, and drafting of the manuscript.

Declaration of interest

The authors have no conflicts of interest, and the publication has not been submitted to any other journal.

Received: May 15, 2020
Revised: September 20, 2020
Accepted: December 11, 2020
Published: January 22, 2021

References

Balaraju, S., Topf, A., McMacken, G., Kumar, V.P., Pechmann, A., Roper, H., Vengalil, S., Polavarapu, K., Nashi, S., Mahajan, N.P., et al. (2020). Congenital myasthenic syndrome with mild intellectual disability caused by a recurrent SLC25A1 variant. Eur. J. Hum. Genet. *28*, 373–377.

Blumkin, L., Halevy, A., Ben-Ami-Raichman, D., Dahari, D., Haviv, A., Sarit, C., Lev, D., van der Knaap, M.S., Lerman-Sagie, T., and Leshinsky-Silver, E. (2014). Expansion of the spectrum of TUBB4A-related disorders: a new phenotype associated with a novel mutation in the TUBB4A gene. Neurogenetics *15*, 107–113.

Brouhard, G.J., and Rice, L.M. (2018). Microtubule dynamics: an interplay of biochemistry and mechanics. Nat. Rev. Mol. Cell Biol. *19*, 451–463.

Cassimeris, L., Silva, V.C., Miller, E., Ton, Q., Molnar, C., and Fong, J. (2012). Fueled by microtubules: does tubulin dimer/polymer partitioning regulate intracellular metabolism? Cytoskeleton (Hoboken) *69*, 133–143.

Consolati, T., Locke, J., Roostalu, J., Chen, Z.A., Gannon, J., Asthana, J., Lim, W.M., Martino, F., Cvetkovic, M.A., and Rappsilber, J. (2020). Microtubule nucleation properties of single human γTuRCs explained by their cryo-EM structure. Dev. Cell *53* (5), 603–617.e8.

Da Palma, M.M., Motta, F.L., Takitani, G., Salles, M.V., Lima, L.H., and Ferraz Sallum, J.M. (2020). TUBGCP4 - associated microcephaly and chorioretinopathy. Ophthalmic Genet. *41*, 189–193.

de Pablo, P.J., Schaap, I.A., MacKintosh, F.C., and Schmidt, C.F. (2003). Deformation and collapse of microtubules on the nanometer scale. Phys. Rev. Lett. *91*, 098101.

Dunlop, R.A., Powell, J.T., Metcalf, J.S., Guillemin, G.J., and Cox, P.A. (2018). L-Serine-Mediated neuroprotection includes the upregulation of the ER stress chaperone protein disulfide isomerase (PDI). Neurotox Res. *33*, 113–122.

Francis, F., and Belvindrah, R. (2018). Tubulin diversity and neuronal migration. Cell Cycle *17*, 405–406.

Fridman, V., Suriyanarayanan, S., Novak, P., David, W., Macklin, E.A., McKenna-Yasek, D., Walsh, K., Aziz-Bose, R., Oaklander, A.L., Brown, R., et al. (2019). Randomized trial of l-serine in patients with hereditary sensory and autonomic neuropathy type 1. Neurology *92*, e359–e370.

Fry, A.M., Sampson, J., Shak, C., and Shackleton, S. (2017). Recent advances in pericentriolar material organization: ordered layers and scaffolding gels. F1000Res *6*, 1622.

Gomez-Ferreria, M.A., Bashkurov, M., Helbig, A.O., Larsen, B., Pawson, T., Gingras, A.C., and Pelletier, L. (2012). Novel NEDD1 phosphorylation sites regulate gamma-tubulin binding and mitotic spindle assembly. J. Cell Sci *125*, 3745–3751.

Hirabayashi, Y., and Furuya, S. (2008). Roles of l-serine and sphingolipid synthesis in brain development and neuronal survival. Prog. Lipid Res. *47*, 188–203.

Hull, S., Arno, G., Ostergaard, P., Pontikos, N., Robson, A.G., Webster, A.R., Hogg, C.R., Wright, G.A., Henderson, R.H.H., Martin, C.A., et al. (2019). Clinical and molecular characterization of familial exudative Vitreoretinopathy associated with microcephaly. Am. J. Ophthalmol. *207*, 87–98.

Jaeken, J., Detheux, M., Van Maldergem, L., Foulon, M., Carchon, H., and Van Schaftingen, E. (1996). 3-Phosphoglycerate dehydrogenase deficiency: an inborn error of serine biosynthesis. Arch. Dis. Child *74*, 542–545.

Jung, Y.K., Han, S.W., Kim, G.W., Jeong, J.H., Kim, H.J., and Choi, J.Y. (2012). DICAM inhibits osteoclast differentiation through attenuation of the integrin alphaVbeta3 pathway. J. Bone Miner Res. *27*, 2024–2034.

Kollman, J.M., Polka, J.K., Zelter, A., Davis, T.N., and Agard, D.A. (2010). Microtubule nucleating gamma-TuSC assembles structures with 13-fold microtubule-like symmetry. Nature *466*, 879–882.

Lawo, S., Bashkurov, M., Mullin, M., Ferreria, M.G., Kittler, R., Habermann, B., Tagliaferro, A., Poser, I., Hutchins, J.R., Hegemann, B., et al. (2009). HAUS, the 8-subunit human Augmin complex, regulates centrosome and spindle integrity. Curr. Biol. *19*, 816–826.

Levine, T.D., Miller, R.G., Bradley, W.G., Moore, D.H., Saperstein, D.S., Flynn, L.E., Katz, J.S., Forshew, D.A., Metcalf, J.S., Banack, S.A., et al. (2017). Phase I clinical trial of safety of L-serine for ALS patients. Amyotroph. Lateral Scler. Frontotemporal Degener *18*, 107–111.

Liebermeister, W., Noor, E., Flamholz, A., Davidi, D., Bernhardt, J., and Milo, R. (2014). Visual account of protein investment in cellular functions. Proc. Natl. Acad. Sci. U S A *111*, 8488–8493.

Liu, J., Ji, X., Li, Z., Zheng, H., Zheng, W., Jia, J., Shen, H., Zhang, Q., and An, J. (2015). Nestin overexpression promotes the embryonic development of heart and brain through the regulation of cell proliferation. Brain Res. *1610*, 1–11.

Loers, G., Liao, Y., Hu, C., Xue, W., Shen, H., Zhao, W., and Schachner, M. (2019). Identification and characterization of synthetic chondroitin-4-sulfate binding peptides in neuronal functions. Sci. Rep. *9*, 1064.

Maver, A., Cuturilo, G., Kovanda, A., Miletic, A., and Peterlin, B. (2019). Rare missense TUBGCP5 gene variant in a patient with primary microcephaly. Eur. J. Med. Genet. *62*, 103598.

Mergenthaler, P., Lindauer, U., Dienel, G.A., and Meisel, A. (2013). Sugar for the brain: the role of glucose in physiological and pathological brain function. Trends Neurosci. *36*, 587–597.

Mingirulli, N., Pyle, A., Hathazi, D., Alston, C.L., Kohlschmidt, N., O'Grady, G., Waddell, L., Evesson, F., Cooper, S.B.T., Turner, C., et al. (2020). Clinical presentation and proteomic signature of patients with TANGO2 mutations. J. Inherit. Metab. Dis. *43*, 297–308.

Mitani, T., Punetha, J., Akalin, I., Pehlivan, D., Dawidziuk, M., Coban Akdemir, Z., Yilmaz, S., Aslan, E., Hunter, J.V., Hijazi, H., et al. (2019). Bi-allelic pathogenic variants in TUBGCP2 cause microcephaly and lissencephaly spectrum disorders. Am. J. Hum. Genet. *105*, 1005–1015.

Miyata, S. (2019). Cytoskeletal signal-regulated oligodendrocyte myelination and remyelination. Adv. Exp. Med. Biol. *1190*, 33–42.

Pasterkamp, R.J., Peschon, J.J., Spriggs, M.K., and Kolodkin, A.L. (2003). Semaphorin 7A promotes axon outgrowth through integrins and MAPKs. Nature *424*, 398–405.

Poli, A., Vial, Y., Haye, D., Passemard, S., Schiff, M., Nasser, H., Delanoe, C., Cuadro, E., Kom, R., Elanga, N., et al. (2017). Phosphoglycerate dehydrogenase (PHGDH) deficiency without epilepsy mimicking primary microcephaly. Am. J. Med. Genet. A *173*, 1936–1942.

Rale, M.J., Kadzik, R.S., and Petry, S. (2018). Phase transitioning the centrosome into a microtubule nucleator. Biochemistry *57*, 30–37.

Raynaud-Messina, B., and Merdes, A. (2007). Gamma-tubulin complexes and microtubule organization. Curr. Opin. Cell Biol. *19*, 24–30.

Romaniello, R., Arrigoni, F., Fry, A.E., Bassi, M.T., Rees, M.I., Borgatti, R., Pilz, D.T., and Cushion, T.D. (2018). Tubulin genes and malformations of cortical development. Eur. J. Med. Genet. *61*, 744–754.

Roos, A., Thompson, R., Horvath, R., Lochmuller, H., and Sickmann, A. (2018). Intersection of proteomics and Genomics to "solve the unsolved" in rare disorders such as neurodegenerative and neuromuscular diseases. Proteomics Clin. Appl. *12*, https://doi.org/10.1002/prca.201700073.

Scheidecker, S., Etard, C., Haren, L., Stoetzel, C., Hull, S., Arno, G., Plagnol, V., Drunat, S., Passemard, S., Toutain, A., et al. (2015). Mutations in TUBGCP4 alter microtubule organization via the gamma-tubulin ring complex in autosomal-recessive microcephaly with chorioretinopathy. Am. J. Hum. Genet. *96*, 666–674.

Scholz-Starke, J., and Cesca, F. (2016). Stepping out of the shade: control of neuronal activity by the scaffold protein Kidins220/ARMS. Front. Cell. Neurosci. *10*, 68.

Seetharaman, S., and Etienne-Manneville, S. (2019). Microtubules at focal adhesions - a double-edged sword. J. Cell Sci. *132*, jcs232843.

Shannon, P., Markiel, A., Ozier, O., Baliga, N.S., Wang, J.T., Ramage, D., Amin, N., Schwikowski, B., and Ideker, T. (2003). Cytoscape: a software environment for integrated models of biomolecular interaction networks. Genome Res. *13*, 2498–2504.

Teixido-Travesa, N., Roig, J., and Luders, J. (2012). The where, when and how of microtubule nucleation - one ring to rule them all. J. Cell Sci. *125*, 4445–4456.

Tovey, C.A., and Conduit, P.T. (2018). Microtubule nucleation by gamma-tubulin complexes and beyond. Essays Biochem. *62*, 765–780.

Vale, R.D. (2003). The molecular motor toolbox for intracellular transport. Cell *112*, 467–480.

Wang, Q., Yang, L., Alexander, C., and Temple, S. (2012). The niche factor syndecan-1 regulates the maintenance and proliferation of neural progenitor cells during mammalian cortical development. PLoS One *7*, e42883.

Wieczorek, M., Urnavicius, L., Ti, S.C., Molloy, K.R., Chait, B.T., and Kapoor, T.M. (2020). Asymmetric molecular architecture of the human gamma-tubulin ring complex. Cell *180*, 165–175 e116.

Wu, J., and Akhmanova, A. (2017). Microtubule-organizing centers. Annu. Rev. Cell Dev. Biol. *33*, 51–75.

Yonezawa, S., Shigematsu, M., Hirata, K., and Hayashi, K. (2015). Loss of gamma-tubulin, GCP-WD/NEDD1 and CDK5RAP2 from the centrosome of neurons in developing mouse cerebral and cerebellar cortex. Acta Histochem. Cytochem. *48*, 145–152.

Yu, N., Signorile, L., Basu, S., Ottema, S., Lebbink, J.H.G., Leslie, K., Smal, I., Dekkers, D., Demmers, J., and Galjart, N. (2016). Isolation of functional tubulin dimers and of tubulin-associated proteins from mammalian cells. Curr. Biol. *26*, 1728–1736.

iScience, Volume *24*

Supplemental Information

Autosomal recessive variants in *TUBGCP2* alter the γ-tubulin ring complex leading to neurodevelopmental disease

Serdal Gungor, Yavuz Oktay, Semra Hiz, Álvaro Aranguren-Ibáñez, Ipek Kalafatcilar, Ahmet Yaramis, Ezgi Karaca, Uluc Yis, Ece Sonmezler, Burcu Ekinci, Mahmut Aslan, Elmasnur Yilmaz, Bilge Özgör, Sunitha Balaraju, Nora Szabo, Steven Laurie, Sergi Beltran, Daniel G. MacArthur, Denisa Hathazi, Ana Töpf, Andreas Roos, Hanns Lochmuller, Isabelle Vernos, and Rita Horvath

Supplementary information

Autosomal recessive variants in *TUBGCP2* alter the γ-tubulin ring complex leading to neurodevelopmental disease

Transparent methods

Whole exome sequencing (WES) and bioinformatics analysis

Patients and family members were recruited at the Department of Paediatric Neurology, Malatya (Turkey) after informed consent. Samples were pseudo-anonymized, processed and stored within the MRC Centre for Neuromuscular Diseases Biobank (National Research Ethics Service, Newcastle and North Tyneside 1 Research Ethics Committee: REC reference number 08/H0906/28+5).

WES of the female patient, parents and the affected brother was performed by the Genomics Platform at the Broad Institute of MIT and Harvard, Cambridge, USA (Yaramis et al., 2020). Libraries were created with an Illumina exome capture (38 Mb target) and sequenced with a mean target coverage of >80x. Genomic and phenotypic data were submitted to the RD-Connect Genome-Phenome Analysis Platform, GPAP, (https://platform.rd-connect.eu), where they can be accessed under a controlled access agreement. Exome sequencing data were processed and analysed on the RD-Connect GPAP. Likely pathogenic variants were identified applying standard filtering for high to moderate variant effect predictor (i.e. nonsense, splice site, frame-shift, in-frame and non-synonymous variants), and for minor allele frequency <1% in gnomAD (http://gnomad.broadinstitute.org), and in a cohort of 1,182 ethnically-matched Turkish control individuals (TUBITAK MAM-GMBE dataset: http://gmbe.mam.tubitak.gov.tr/en). Shortlisted variants were interrogated for their predicted *in silico* deleteriousness, previous known association with human disease and were

classified by the ACMG Guidelines. Likely pathogenic variants were segregated in unaffected siblings by Sanger sequencing. All exome data are available in the RD-CONNECT platform.

Analysis of components of γ-TuRC

Immunofluorescence images were taken of human fibroblasts grown on coverslips and MetOH fixed. Permeabilization and blocking of fibroblasts was carried out in IF buffer (0,5% BSA, 0,1% Triton X-100 in PBS) for 30 min at RT. After blocking and permeabilization, human fibroblasts were incubated with primary antibodies diluted in IF buffer for 1 h at RT and then 3 washes of 5 min in IF buffer were performed. Samples were then incubated with secondary antibodies for 45 min at RT and washed once with IF buffer and twice with PBS. Antibodies and concentrations were the following: mouse anti-γ-tubulin (1:1000, Sigma, T6199), rabbit anti-PCTN (1:500, Abcam, Ab4448), rabbit anti-HAUS6 (1:2000, Homemade), anti-NEDD1 (1:1500, Abnova, H00121441-M05), mouse anti-α-tubulin (1:1000, Sigma, T9026), rabbit anti-β-tubulin (1:350, Abcam, Ab6046).

For western blot analysis, human fibroblasts were synchronized with a double thymidine (2 mM, overnight) nocodazole (0,33 uM, overnight) block and then lysed in lysis buffer (50 mM Tris-HCl pH 7,4, 150 mM NaCl, 1% NP-40, 1 mM EDTA and protease inhibitors). 30 ug of total cell lysates were subjected to 8% SDS-PAGE and blotted onto nitrocellulose membranes (Millipore). Membranes were blocked with 3% BSA in TBS-Tween 0,1% (TBS-T 0,1%) for 45 min, rinsed in distilled water and probed with the following primary antibodies diluted in TBS-T 0,1%, 0,5% BSA for 1 h at RT: rabbit anti-TUBGCP2 (1/2000, Homemade), rabbit anti-TPX2 (1 ug/ml, Homemade), mouse anti-acetylated tubulin (1:1000, Sigma, T7451), rabbit anti-β-tubulin (1:1000, Abcam, Ab6046). After primary antibody incubation and 3 washes of 5 min in TBS-T 0,1%, membranes were incubated for 45 min at RT with the following secondary

antibodies diluted in TBS-T0,1%, 0,5% BSA: goat anti-rabbit irDye 800CW (1:20000, Fisher Scientific, 10733944) and goat anti-mouse Alexa Fluor™ 680 (1:20000, Invitrogen, A21058) . After secondary antibody incubation, membranes were washed three times with TBS-T 0,1% and subjected to developing using the Oddysey infrared imaging system. The signal intensity of the γ-TuRC components in mitosis was measured using Fiji software, normalized to the tubulin signal intensity and represented in a scatter plot.

Structural Modelling of the *TUPBGCP2* missense mutation

The structural modeling of GCP2_E311K:GCP3 complex was carried out with the HADDOCK web server (https://haddock.science.uu.nl/services/HADDOCK2.2/ (Vangone et al., 2017) by using chains C and D of the γ-TuRC ring complex as a template (pdb id: 6v6s). A similar mutation modeling procedure was described in Dafsari *et al.* (Dafsari et al., 2019). To generate the electrostatic surfaces: (i) the relevant .pqr files were calculated with the http://server.poissonboltzmann.org/ server (Dolinsky et al., 2004), (ii) the acquired .pqr distributions were visualized with the APBS plugin of PyMOL.

Proteomic Profiling

Sample preparation and trypsin digestion

In total seven samples (fibroblasts) derived from 4 healthy controls (gender and age-matched) and from one TUBGCP patients (processed and measured in triplicates) were processed independently. After harvesting cells were lysed in 500 µL of lysis buffer (50 mM Tris-HCl (Applichem Biochemica A3452) (pH 7.8) 150 mM NaCl, 1 % SDS (Carl Roth CN30.1), and Complete Mini Roche 11873580001) and treated with Benzonaze (Sigma-Aldrich) for 30

minutes at 37°C in order to degrade the DNA. Then samples were centrifuged for 5 min at 4°C and 5000 *g*. Protein concentration of the supernatant was determined by BCA assay (ThermoFisher 23225) (according to the manufacturer's protocol) and cysteines were reduced with 10 mM of DTT (Roche 10708984001) by incubation at 56°C for 30 min. Next, the free thiol groups were alkylated with 30 mM IAA (Sigma-Aldrich I1149-25G) at room temperature (RT) in the dark for 30 minutes. Sample cleanup and proteolysis were performed using filter-aided sample preparation (FASP) as described previosuly (Mingirulli et al., 2020) . Briefly, 100 µg of protein was diluted 10-fold with freshly prepared 8M urea (Sigma-Aldrich)/100mM Tris-HCl (Applichem Biochemica) (pH 8.5) buffer and placed on a centrifugal device Nanosep 30 kDa Omega (Merck). The device was centrifuged at 13,800 g at RT for 20 min for all centrifugation steps. First, to eliminate residual SDS, three washing steps were carried out with 100 µL of 8M urea (Sigma-Aldrich) /100mM Tris-HCl (Applichem Biochemica) (pH 8.5). Then, for buffer exchange, the device was washed thrice with 100 µL of 50mM NH4HCO3 (Sigma-Aldrich S2889-250G) (pH 7.8). Next, 100 µL of proteolysis buffer comprising of trypsin (Promega) (1:25 w/w, protease to substrate), 0.2M GuHCl (Sigma-Aldrich) and 2mM CaCl2 ((Sigma-Aldrich)) in 50mM NH4HCO3 (Sigma-Aldrich) (pH 7.8), was added to the device and incubated at 37 °C for 14 h. Afterwards, the generated tryptic peptides were recovered by centrifugation with 50 µL of 50mM NH4HCO3 (Sigma-Aldrich) followed by 50 µL of ultra-pure water. Finally, peptides were acidified ((pH<3) by addition of 10% TFA (Biosolve) (v/v) and digests were quality-controlled in a reversed-phase HPLC as described previously (Mingirulli et al., 2020).

LC-MS/MS analysis

Samples (1 µg) were analyzed using an Ultimate 3000 nano RSLC system coupled to an LTQ Orbitrap Velos mass spectrometer (both Thermo Scientific). Peptides were preconcentrated

on a 75 µm x 2 cm C18 trapping column for 16 min using 0.1 % TFA (v/v) with a flow rate of 20 µl/min followed by separation on a 75 µm x 50 cm C18 main column (both Pepmap, Thermo Scientific) with a 130 min LC gradient ranging from 3-38 % ACN in 0.1 % FA (v/v) at a flow rate of 250 nl/min. MS survey scans were acquired in the Orbitrap from m/z 300 to 1500 at a resolution of 60,000 using the polysiloxane ion at *m/z* 371.101236 as lock mass. Theten most intense signals were subjected to collision induced dissociation (CID) in the ion trap taking into account a dynamic exclusion of 25 s. CID spectra were acquired with a normalized collision energy of 35 %. AGC target values were set to 10^6 for Orbitrap MS and 10^4 for ion trap MS^n scans.

Label free data analysis

Label free quantification of the acquired MS data was performed using the Progenesis LC-MS software from Nonlinear Dynamics (Newcastle upon Tyne, U.K.). Raw files were imported and the alignment of the MS runs was done automatically by the software by choosing one of the runs as reference. After peak picking, only features within retention time and m/z windows 0-130 min and 300-1500, respectively, and with charge states +2, +3 and +4 were considered for peptide statistics, analysis of variance (ANOVA) and principal component analysis (PCA). Spectra were exported as peak lists and searched against a concatenated target/decoy version of the human Uniprot database, (downloaded on 22.07.2015 containing 20273 target sequences) using Mascot 2.4 (Matrix Science), MS-GF+ and X!Tandem (version 2013.02.01.1) with the help of searchGUI 3.2.5 (Vaudel et al., 2011). Trypsin with a maximum of two missed cleavages was selected as enzyme. Carbamidomethylation of Cys was set as fixed, acetylation of protein N-terminus, oxidation of Met and phosphorylation of Ser/Thr/Tyr were selected as variable modifications. MS and MS/MS tolerances were set to 10 ppm and 0.5 Da, respectively. Search results were combined at a false discovery rate (FDR) of 1 % on the protein level using

the PeptideShaker software 1.4.0 (http://code.google.com/p/peptide-shaker/) and processed for re-import as peptide spectrum matches into Progenesis. Finally, 1681 proteins which were quantified from the non-conflicting features (i.e. only unique peptides) were exported. For all proteins, the normalized abundances from Progenesis were used to calculate standard deviations (SD) and coefficients of variation (CV) using all three replicates per condition. Only proteins with a p-value <0.05 and showing an average ratio <0.45 or >2.28 were considered as regulated.

TUBGCP2 expression in human skin fibroblasts was investigated by screening a protein/ spectral library covering 96,512 peptides referring to 8234 proteins expressed in these cells (Hentschel et al., preprint available DOI: 10.21203/rs.3.rs-48014/v1) for tryptic peptides unique for TUBGCP2.

Immunofluorescence studies on human skin fibroblasts

Immunofluorescence studies on human skin fibroblasts were carried out as following: cells were grown to a confluency of 60% on cover slips in a 24-well plate, washed twice with PBS, fixed with 4% formalin in PBS for 15 min and after the fixative was aspirated, cells were washed again twice with PBS. To quench the free aldehyde groups of the fixative, 10 mM NH_4Cl-PBS was added to the cells and incubated for 15 min. After fibroblasts were washed two times with PBS, they were permeabilized by adding 0.5 ml 0.1% Triton X-100 (in PBS) to each well (incubation for 10 min). Next, blocking was carried out by adding 100 µl 1% BSA made in PBS containing 0.1% Triton X-100 (v/v) to each well. Primary antibodies (α-CD63: ab8219, α-aB-Crystallin: sc-137129, α-Desmin: NCL-L-DES-DERII, α-PHGDH: GTX101948, Phalloidin: ab176753, α-Tenascin: AB19011) were diluted in 1% BSA blocking solution made in PBS containing 0.1% Triton X-100 (v/v) and incubated for one hour at room temperature. After

antibody solutions were aspirated and fibroblasts were washed with PBS containing 0.1% Triton X-100 secondary antibodies (Invitrogen Alexa488 & Alexa594) diluted 1:500 in 1% BSA blocking solution made in PBS containing 0.1% Triton X-100 (v/v) were added and incubated for one hour at room temperature. In the following step, antibody solutions were aspirated, and fibroblasts washed twice with PBS containing 0.1% Triton X-100. For mounting, 10 µl mounting medium (containing anti-fade reagent) was placed on the slide for each coverslip and coverslips were positioned at the centre of the slide. Excess of mountant was drawn with filter paper and mounting medium was solidified for two hours before samples were examined on microscope (Zeiss Axioplan).

Investigation of cellular fitness

To measure cellular metabolic activity as an indicator of cell viability, proliferation and cytotoxicity, the MTT-assay (Sigma, M5655-100MG) was applied to TUBGCP2-patient derived and control fibroblasts treated and non-treated with 80 µm L-serine (Sigma, S4311-25G), respectively. Viable cells contain NAD(P)H-dependent oxidoreductase enzymes which reduce the MTT to formazan; the insoluble formazan crystals are dissolved using a solubilization solution and the resulting coloured solution is quantified by measuring absorbance at 500-600 nanometers using a multi-well spectrophotometer (Tecan Infinity 200). Here, the darker the solution, the greater the number of viable, metabolically active cells. The assay was carried out according to manufacturer's specifications.

Supplementary Figures and Table

Supplementary Figure 1 (related to Figure 5) shows Violin plots depicting tissue/cell expression of TUBGCP2 from GTEx Portal (https://gtexportal.org/home/gene/TUBGCP2) **illustrate high expression in neuronal cell types, but also in cultured skin fibroblasts.**

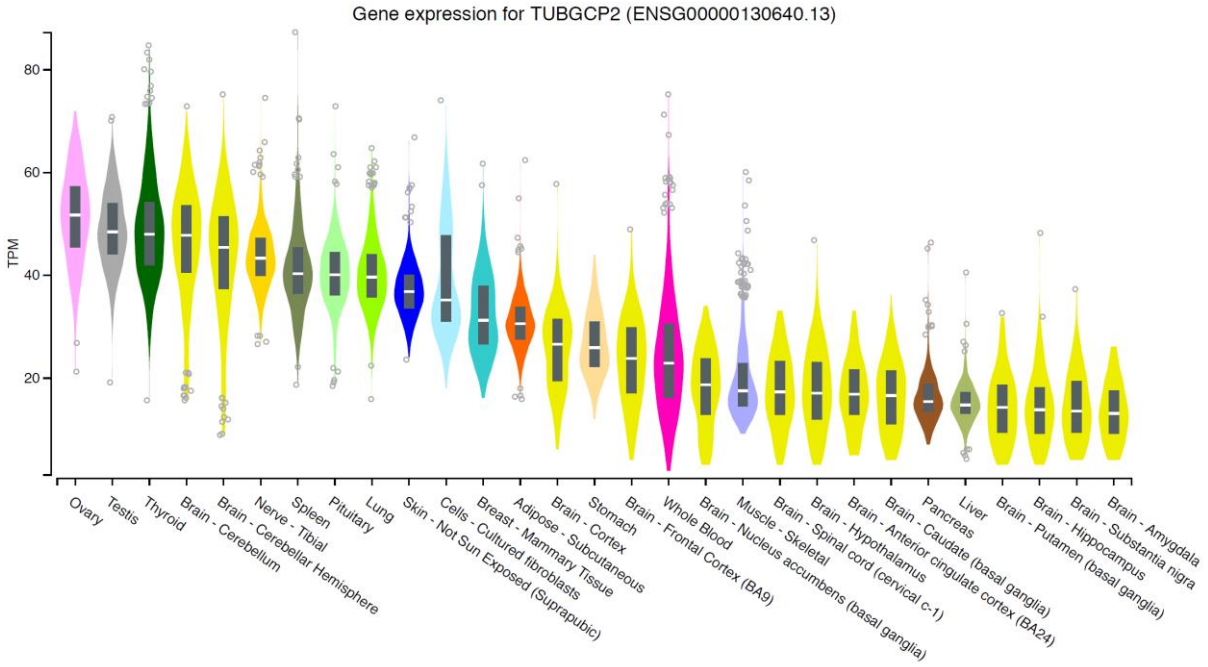

Supplementary Figure 2 (related to Figure 5). Protein targets of TUBGCP2 used in our proteomics studies (bold highlighted, p.E311K red).

>sp|Q9BSJ2|GCP2_HUMAN Gamma-tubulin complex component 2 OS=Homo sapiens OX=9606 GN=TUBGCP2 PE=1 SV=2

MSEFRIHHDVNELLSLLRVHGGDGAEVYIDLLQKNRTPYVTTTVSAHSAKVKIAEFSRTPEDFLKKYDELKSKNTR**NL**
DPLVYLLSKLTEDKETLQYLQQNAKERAELAAAAVGSSTTSINVPAAASKISMQELEELRK**QLGSVATGSTLQQSLEL**
KRKMLRDKQNKKNSGQHLPIFPAWVYERPALIGDFLIGAGISTDTALPIGTLPLASQESAVVEDLLYVLVGVDGRYVS
AQPLAGRQSR**TFLVDPNLDLSIR**ELVHR**ILPVAASYSAVTR**FIEEK**SSFEYGQVNHALAAAMR**TLVKEHLILVSQLEQ
LHRQGLLSLQKLWFYIQPAMRTMDILASLATSVDKGECLGGSTLSLLHDRSFSYTGDSQAQELCLYLTK**AASAPYFEV**
LEKWIYRGIIHDPYSEFMVEEHELRKER**IQEDYNDKYWDQRYTIVQQQIPSFLQK**MADKILSTGKYLNVVR**ECGHD**
VTCPVAKEIIYTLKERAYVEQIEKAFNYASKVLLDFLMEEKELVAHLRSIKRYFLMDQGDFFVHFMDLAEEELRKPVED
ITPPRLEALLELALR**MSTANTDPFKDDLK**IDLMPHDLITQLLRVLAIETKQEKAMAHADPTELALSGLEAFSFDYIVKW
PLSLIINRKALTRYQMLFRHMFYCKHVERQLCSVWISNKTAKQHSLHSAQWFAGAFTLRQRMLNFVQNIQYYMM
FEVMEPTWHILEKNLKSASNIDDVLGHHTGFLDTCLKDCMLTNPELLKVFSKLMSVCVMFTNCMQKFTQSMK**LDG**
ELGGQTLEHSTVLGLPAGAEERARKELARKHLAEHADTVQLVSGFEATINKFDKNFSAHLLDLLAR**LSIYSTSDCEHG**
MASVISRLDFNGFYTERLERLSAERSQKATPQVPVLRGPPAPAPRVAVTAQ

Supplementary Table 1 (related to Figure 5) shows the list of differentially regulated proteins in *TUBGCP2* mutant fibroblasts.

Uniprot Accession #	Protein name	Gene name	#Peptides	Fold change	Anova (p)	Protein function
Q9UKX5	Integrin alpha-11	*ITA11*	4	4.21	<0.0005	Receptor for collagen
Q08431	Lactadherin	*MFGM*	2	3.58	<0.0005	Essential role in neurons in Aβ-induced phagoptosis
P52943	Cysteine-rich protein 2	*CRIP2*	2	3.46	<0.0005	Invadopodia actin bundling factor
P02511	Alpha-crystallin B chain	*CRYAB*	8	3.27	<0.0005	Chaperone-like activity, preventing aggregation of various proteins
P17661	Desmin	*DESM*	4	3.24	<0.0005	Act as a (sarcomeric) microtubule-anchoring protein: specifically associates with detyrosinated tubulin-alpha chains, leading to buckled microtubules
Q6UVK1	Chondroitin sulfate proteoglycan 4	*CSPG4*	15	2.79	<0.0005	Inhibits neurite outgrowth and growth cone collapse during axon regeneration; cell surface receptor for collagen alpha 2(VI)
Q8TAD7	Overexpressed in colon carcinoma 1 protein	*OCC1*	3	2.74	<0.0005	
Q14699	Raftlin	*RFTN1*	2	2.64	<0.0005	Involved in protein trafficking; mediates internalization of TLR4 to endosomes in dendritic cells
P55290	Cadherin-13	*CAD13*	6	1.40	<0.0005	Acts as a negative regulator of neural cell growth
O75326	Semaphorin-7A	*SEM7A*	4	1.35	<0.0005	Plays an important role in integrin-mediated signaling and functions; promotes axon growth in the embryonic olfactory bulb. Promotes attachment, spreading and dendrite outgrowth
Q14108	Lysosome membrane protein 2	*SCRB2*	3	2.38	<0.0005	Lysosomal receptor for glucosylceramidase (GBA) targeting
Q15149	Plectin	*PLEC*	219	2.34	<0.0005	Interlinks intermediate filaments with microtubules and microfilaments and anchors intermediate filaments to desmosomes or hemidesmosomes. Could also bind muscle proteins such as actin to membrane complexes in muscle
Q8TF66	Leucine-rich repeat-containing protein 15	*LRRC15*	1	10.66	<0.0005	Promotes osteogenic differentiation of mesenchymal stem cells
O94907	Dickkopf-related protein 1	*DKK1*	1	7.74	<0.0005	Inhibit Wnt regulated processes such as antero-posterior axial patterning, somitogenesis and eye formation; in adults implicated in bone formation cancer and Alzheimer disease
Q9Y6U3	Adseverin	*ADSV*	1	4.10	<0.0005	Ca^{2+}-dependent actin filament-severing protein that has a regulatory function in exocytosis by affecting the organization of the microfilament network underneath the plasma membrane
Q96LJ7	Dehydrogenase/reductase SDR family member 1	*DHRS1*	1	3.85	<0.0005	NADPH-dependent reductase that is able to catalyse the in vitro reductive conversion of some steroids
O94919	Endonuclease domain-containing 1 protein	*ENDOD1*	1	3.20	<0.0005	Act as a DNase and a RNase

Q9ULH0	Kinase D-interacting substrate of 220 kDa	*KDIS*	1	3.11	<0.0005	Plays a role in nerve growth factor (NGF)-induced recruitment of RAPGEF2 to late endosomes and neurite outgrowth. May play a role in neurotrophin- and ephrin-mediated neuronal outgrowth and in axon guidance during neural development and in neuronal regeneration
Q5JRX3	Presequence protease (mitochondrial)	*PREP*	1	2.78	<0.0005	Metalloendopeptidase of the mitochondrial matrix that functions in peptide cleavage and degradation
Q96HC4	PDZ and LIM domain protein 5	*PDLI5*	1	2.76	0.01	Actin binding protein which plays an important role in the heart development by scaffolding PKC to the Z-disk region; overexpression promotes the development of heart hypertrophy
Q9BRK3	Matrix-remodeling-associated protein 8	*MXRA8*	1	2.74	<0.0005	Modulates activity of various signaling pathways, probably via binding to integrin
P16402	Histone H1.3	*H1-3*	1	2.67	<0.0005	Binds to linker DNA between nucleosomes and acts as a regulator of individual gene transcription through chromatin remodeling
Q14956	Transmembrane glycoprotein NMB	*GPNMB*	1	2.65	<0.0005	Activator of the ERK1/2 and Akt pathways toward the prevention of build-up of TDP-43 aggregates
P18827	Syndecan-1	*SDC1*	1	2.50	0.01	Cell surface proteoglycan that links the cytoskeleton to the interstitial matrix and regulates exosome biogenesis
O75521	Enoyl-CoA delta isomerase 2 (mitochondrial)	*ECI2*	1	2.30	<0.0005	Isomerizes both, 3-cis and 3-trans double bonds into the 2-trans form in a range of enoyl-CoA species
P48061	Stromal cell-derived factor 1	*CXCL12*	1	2.29	0.02	Induces migration of oligodendrocyte precursor cells through activated ERK and AKT pathways
P02461	Collagen alpha-1(III) chain	*CO3A1*	19	0.45	<0.0005	Involved in regulation of cortical development; major ligand of ADGRG1 in the developing brain and binding to ADGRG1 inhibits neuronal migration and activates the RhoA pathway
Q15063	Periostin	*POSTN*	3	0.45	<0.0005	Induces cell attachment and spreading and plays a role in cell adhesion
P55957	BH3-interacting domain death agonist	*BID*	1	0.45	0.01	Initiates apoptosis
Q7Z434	Mitochondrial antiviral-signaling protein	*MAVS*	1	0.45	<0.0005	MAVS signaling activation causes induction of autophagic activation in brain
P40261	Nicotinamide N-methyltransferase	*NNMT*	6	0.45	<0.0005	Protectant against neurotoxin-mediated cell death; increased expression promotes neurite branching, synaptophysin expression and dopamine accumulation and release
O43175	D-3-phosphoglycerate dehydrogenase	*PHGDH*	16	0.42	<0.0005	Modulates first step of the phosphorylated L-serine biosynthesis pathway
Q9Y613	FH1/FH2 domain-containing protein 1	*FHOD1*	1	0.42	<0.0005	Contributes to the coordination of microtubules with actin fibers and plays a role in cell elongation
O14495	Lipid phosphate phosphohydrolase 3	*LPP3*	3	-1.28	<0.0005	Involved in cell adhesion and in cell-cell interactions; lack in embryonic stem cells compromises neuronal differentiation and neurite outgrowth

Q02952	A-kinase anchor protein 12	*AKA12*	17	-1.33	<0.0005	Anchoring protein that mediates the subcellular compartmentation of protein kinase A (PKA) and protein kinase C (PKC)
P22692	Insulin-like growth factor-binding protein 4	*IGFBP4*	2	-1.37	<0.0005	Inhibits proliferation and promotes differentiation of neural progenitor cells
P60174	Triosephosphate isomerase	*TPIS*	20	-1.37	<0.0005	Reduced function of this protein triggers neuronal death
Q9BRA2	Thioredoxin domain-containing protein 17	*TXNDC17*	3	-1.38	<0.0005	Disulfide reductase; modulates TNF-alpha signaling and NF-kappa-B activation
P10620	Microsomal glutathione S-transferase 1	*MGST1*	3	-1.39	<0.0005	Conjugation of reduced glutathione to a wide number of exogenous and endogenous hydrophobic electrophiles
Q16647	Prostacyclin synthase	*PTGIS*	6	-1.41	<0.0005	Catalyzes the isomerization of prostaglandin H2 to prostacyclin
P24821	Tenascin	*TENA*	24	-1.52	0,01	Extracellular matrix protein implicated in guidance of migrating neurons as well as axons during development, synaptic plasticity as well as neuronal regeneration. Promotes neurite outgrowth from cortical neurons
P52209	6-phosphogluconate dehydrogenase, decarboxylating	*PGD*	8	-1.70	<0.0005	Catalyzes the oxidative decarboxylation of 6-phosphogluconate to ribulose 5-phosphate and CO_2
P48681	Nestin	*NEST*	8	-1.70	<0.0005	Required for brain and eye development. Promotes the disassembly of phosphorylated vimentin intermediate filaments (IF) during mitosis and may play a role in the trafficking and distribution of IF proteins and other cellular factors to daughter cells during progenitor cell division. Required for survival, renewal and mitogen-stimulated proliferation of neural progenitor cells
Q15392	Delta(24)-sterol reductase	*DHC24*	2	0.29	<0.0005	Protects cells from oxidative stress; protects against amyloid-beta peptide-induced apoptosis
Q93062	RNA-binding protein with multiple splicing	*RBPMS*	2	-2.29	<0.0005	Acts as a coactivator of transcriptional activity
P53634	Dipeptidyl peptidase 1	*CATC*	3	-2.43	<0.0005	Activates serine proteases such as elastase, cathepsin G and granzymes A and B; can also activate neuraminidase
P24593	Insulin-like growth factor-binding protein 5	*IGFBP5*	2	-4.69	<0.0005	Inhibitory binding protein for insulin-like growth factor 1; overexpression leads to motor axonopathy and sensory deficits in mice
P54826	Growth arrest-specific protein 1	*GAS1*	1	0.03	0.04	Specific growth arrest protein involved in growth suppression; blocks entry to S phase; promotes neurite outgrowth
Q8NDI1	EH domain-binding protein 1	*EHBP1*	1	-2.00	0.01	Plays a role in actin reorganization; links clathrin-mediated endocytosis to the actin cytoskeleton; May act as Rab effector protein and play a role in vesicle trafficking
P26022	Pentraxin-related protein PTX3	*PTX3*	1	-6.20	<0.0005	Plays a protective role in seizure-induced neurodegeneration

References

Dafsari, H.S., Sprute, R., Wunderlich, G., Daimaguler, H.S., Karaca, E., Contreras, A., Becker, K., Schulze-Rhonhof, M., Kiening, K., Karakulak, T.*, et al.* (2019). Novel mutations in KMT2B offer pathophysiological insights into childhood-onset progressive dystonia. J Hum Genet *64*, 803-813.

Dolinsky, T.J., Nielsen, J.E., McCammon, J.A., and Baker, N.A. (2004). PDB2PQR: an automated pipeline for the setup of Poisson-Boltzmann electrostatics calculations. Nucleic Acids Res *32*, W665-667.

Mingirulli, N., Pyle, A., Hathazi, D., Alston, C.L., Kohlschmidt, N., O'Grady, G., Waddell, L., Evesson, F., Cooper, S.B.T., Turner, C.*, et al.* (2020). Clinical presentation and proteomic signature of patients with TANGO2 mutations. J Inherit Metab Dis *43*, 297-308.

Vangone, A., Rodrigues, J.P., Xue, L.C., van Zundert, G.C., Geng, C., Kurkcuoglu, Z., Nellen, M., Narasimhan, S., Karaca, E., van Dijk, M.*, et al.* (2017). Sense and simplicity in HADDOCK scoring: Lessons from CASP-CAPRI round 1. Proteins *85*, 417-423

Vaudel, M., Barsnes, H., Berven, F.S., Sickmann, A., and Martens, L. (2011). SearchGUI: An open-source graphical user interface for simultaneous OMSSA and X!Tandem searches. Proteomics *11*, 996-999.